DMD Fast Forward. Published on November 4, 2009 as doi:10.1124/dmd.109.029843

DMD 29843

If the K_I is defined by the free energy of binding to P-gp, which kinetic parameters define the IC50 for the MDCKII-hMDR1 confluent cell monolayer?

Annie Albin Lumen[#], Poulomi Acharya[#,&], Joseph W. Polli, Andrew Ayrton, Harma Ellens and Joe Bentz

Department of Biology, Drexel University, Philadelphia, PA 19104 (A.A.L., P.A., J.B.)

Preclinical Drug Metabolism and Pharmacokinetics, GlaxoSmithKline, King of Prussia, PA (A.A.L., P.A., H.E.)

Preclinical Drug Metabolism and Pharmacokinetics, GlaxoSmithKline, Research Triangle Park, NC 27709 (J.W.P.)

Preclinical Drug Metabolism and Pharmacokinetics, GlaxoSmithKline, Welwyn, England (A.A.)

Running Title: The $IC50/K_I$ ratio for a confluent cell monolayer

Address correspondence to:

Dr. Joe Bentz, Dept. of Biology, Drexel University, 32nd& Chestnut Sts., Philadelphia, PA, 19104, Phone: 215-895-1513, email: bentzj@drexel.edu, FAX: 215-895-1273.

Main Text Pages: (pp 4 to 25)=22 pages

Figures: 13

Tables: 2

References: 40

Abstract word count: 210 (Max limit = 250)

Introduction word count: 572 (Max limit = 750)

Discussion word count: 1465(Max limit = 1500)

Supplementary Data (pp 1-24)=24 pages

Non-standard Abbreviations: P-gp, the P-glycoprotein product of the hMDR1 gene; A>B (or B>A), transport across the confluent cell monolayer when the donor chamber is apical (or basolateral) and the receiver chamber is basolateral (or apical) respectively; K_C is the substrate binding constant to P-gp relative to the lipid bilayer; $K_D=1/(K_C K_{PC})$ is the substrate dissociation constant from P-gp relative to the aqueous concentration in the cytosol, where K_{PC} is the substrate's equilibrium partition coefficient into the cytosolic side of the apical memebrane; K_I is the K_D of a P-gp substrate when it is used as an inhibitor.

Abstract

From previous fits of drug transport kinetics across confluent MDCKII-hMDR1 cell monolayers, we found that a drug's binding constant to P-gp was significantly smaller than its IC50 when that drug was used as an inhibitor against another P-gp substrate. We tested several IC50 candidate functions, including the standard function, the Kalvass-Pollack function and the efflux ratio, to determine whether any of them yielded an $IC50=K_I$, as would be expected for water soluble enzymes. For the confluent cell monolayer, the $IC50/K_I$ ratio is greater than 1 for all candidate functions tested. From the mass action kinetic model, we have derived a simple approximate equation that shows how the $IC50/K_I$ ratio depends upon the elementary rate constants from our mass action model. Thus, the IC50 will differ between cell lines and tissues, for the same probe-substrate and inhibitor, if there are different membrane concentrations of P-gp, or the probe substrate's elementary rate constants, partition coefficient, binding constant to P-gp, passive permeability and its ability to access the other transporters(if any) in the two cell lines. The mass action model and the approximate equation for the $IC50/K_I$ ratio derived here can be used to estimate the elementary rate constants needed to extrapolate in vitro drug-drug interactions for compounds to the in vivo environment.

Introduction

The importance of membrane transporters in the metabolism and disposition of drugs is clear (Chang and Benet, 2005; Collett et al, 2005; Endres et al, 2006; Shitara et al, 2006; Bartholome et al., 2007; Balimane et al., 2008; Glavinas et al., 2008; Kurnik et al., 2008; Nies et al., 2008). Assessing drug-drug interaction risk is an important aspect of drug development, which is often quantified by the concentration of inhibitor required to reduce probe-substrate transport by 50%, reported as the IC50 (Gao et al, 2001; Zong and Pollack, 2003; Rautio et al, 2006). The basic function of the IC50 experiment is to rank order compounds with respect to inhibition of the probe substrate transport and then to use this list along with other relevant clinical information to predict *in vivo* activity. The IC50 is usually assumed to be a fairly good estimate of the true thermodynamic dissociation constant of the inhibitor, K_I, to the transporter.

For a 1-site enzyme that competitively binds both drug and inhibitor directly from the aqueous phase, the ratio of $IC50/K_I=1+K_C[L]$, where [L] is the probe-substrate concentration and K_C is the probe-substrate binding constant (Cheng and Prusoff, 1973). This equation should work for membrane transporters that bind their substrate directly from the extracellular phase, e.g. glucose permeases (Hah et al, 2002).

For transporters that bind drug from the inner monolayer of the plasma membrane, such as P-gp (Loo and Clarke, 2005; Lugo and Sharom, 2005) and MRP (Borst et al, 2006), the binding site is a permeability barrier away from where the drug is added. Drug concentration at the binding site within the apical membrane depends upon the partition coefficient of the drug to the inner apical membrane. At a minimum, this suggests that passive permeability through the plasma membrane and the partition coefficient should influence the $IC50/K_I$ ratio. We have already shown when

the steady-state Michaelis-Menten equations are used to analyze P-gp mediated transport of a substrate through the confluent cell monolayer that the fitted Michaelis constant Km depends upon the passive-permeability of the substrate through the membranes (Bentz et al, 2005).

We previously fitted the elementary rate constants for substrate binding to P-gp and efflux from P-gp for amprenavir, digoxin, loperamide and quinidine, using an MDCKII-hMDR1 cell monolayer, see Table 1 (Tran et al, 2005; Acharya et al, 2006, 2008). As expected, each of these P-gp substrates inhibited the transport of the other P-gp substrates (Acharya et al, 2006). However, we discovered that the IC50's we measured experimentally, which agree with Rautio et al. (2006), were much larger than the K_I predicted using our fitted dissociation constants and partition coefficients of the inhibitors, even at very low substrate concentrations.

In this work, we explain the source of the difference between an IC50 and a K_I in the confluent cell system with experiments and our mass action model. We have derived a simple approximate equation from the mass action model for the $IC50/K_I$ ratio in terms of the elementary rate constants for the probe-substrate and the inhibitor. Our nonlinear mass action model is more difficult to solve than the standard Michaelis-Menten models (Ho et al., 2000; Bartholome et al., 2007; Sun and Pang, 2008), but we obtain a deeper understanding of how transport through the confluent cell monolayer works, which cannot be extracted from the simpler steady-state kinetic models. Thus, in vitro extrapolations to in vivo are more reliable when launched from this nonlinear mass action model.

Materials and Methods

Compounds: Amprenavir and GF120918 were from GlaxoSmithKline; loperamide and quinidine were from Sigma (St. Louis, MO). ^{3}H-amprenavir (24 Ci/mmol) was custom-synthesized by Amersham Pharmacia Biotech, U.K. ^{3}H-quinidine (20 Ci/mmol) was from American Radiolabelled Chemicals Inc. (St. Louis, MO). Dimethyl sulfoxide (DMSO) was from Sigma-Aldrich (St. Louis, MO). Dulbecco's modified Eagle's medium (DMEM) with 25 mM *N*-2-hydroxyethylpiperazine-*N*'-2-ethanesulfonic acid (HEPES) buffer, high glucose (4.5 g/L), L-glutamine, pyridoxine hydrochloride, without sodium pyruvate, and with phenol red was from Gibco (Grand island, NY). The same medium without phenol red was used for transport experiments. Transwell 12-well plates with polycarbonate inserts (0.4 μM pore size and 12 mm in diameter) were obtained from Costar (Acton, MA).

Experimental Methods.

Cell Line and Culture Conditions. The Madin-Darby Canine Kidney II cell line over-expressing human MDR1 (MDCKII_hMDR1) was obtained from The Netherlands Cancer Institute (Amsterdam, The Netherlands). The cells were grown in 175 cm^2 culture flasks using DMEM with 10% fetal bovine serum, 1% L-glutamine, 50 units/mL penicillin, and 50 mg/mL streptomycin at 37°C in 5% CO_2 atmosphere. Cells were split in a ratio of 1:40 twice a week at 70-80% confluency after at least 2 washes with PBS and trypsinization with 0.25% trypsin/ethylenediaminetetraacetic acid (EDTA). All transport assays were performed with cells from passages 30 to 55.

Inhibition Studies. Cell monolayers were preincubated for 1 hour with inhibitor-containing transport medium in both apical and basolateral chambers. After preincubation, fresh media with appropriate inhibitor concentration was added to both basolateral and apical chamber along with the radiolabeled substrate on the chosen donor side. After a 4 hour incubation period, samples were taken from both apical and basolateral chambers and counted using a TopCount Model 9912. Passive permeability of the substrate was determined in the presence of 2uM GF120918. Lucifer yellow was added to the apical chambers in all cases to assess monolayer integrity. Other details are described in Acharya et al. (2006, 2008).

Simulations. For all drugs tested, there is an initial increase in the passive permeability coefficients followed by a true steady-state (Tran et al, 2005; Acharya et al, 2006). For the simulations in this work, these transients will be ignored and the monolayers treated as static passive permeability barriers where passive permeability coefficients are constant in time. Including these transients would only increase the IC50 overestimate of the K_I.

In permeability studies with cell monolayers, it is only possible to measure transport across the entire monolayer, which yields the passive permeability coefficients P_{BA}, basolateral to apical chamber, and P_{AB}, apical to basolateral chamber. However, for fitting the mass action kinetics, other individual membrane passive permeability coefficients are needed, including P_{AC}, apical chamber to cytosol, and P_{BC}, basolateral chamber to cytosol. Another challenge to these simulations is that often P_{BA} does not equal P_{AB} until a true steady-state occurs (Tran et al, 2005; Acharya et al, 2006). The simplest mix of experiment and theory is to set $P_{AC} = P_{CA} = P_{AB}$ and $P_{BC} = P_{CB} = P_{BA}$ to account for this asymmetry and to capture the basic elements of the observed kinetic process. See Tran et al. (2005) for more details. We used the stiffest integrator in MATLAB, ode23s, with absolute and relative tolerances set up to 10^{-8}.

Kinetic Model of Transport across a Confluent Cell Monolayer

Figure 1 is a cartoon of a confluent cell monolayer, featuring the polarized MDCKII-hMDR1 cells, where the basolateral membrane is attached to the polycarbonate filters and P-gp (upward arrows) is expressed on the apical surface. The apical and basolateral chambers are kept separate by the tight junctions. Active transport by P-gp occurs unidirectionally, with substrate binding to a site on P-gp within the apical membrane inner monolayer and with efflux into the apical chamber (Loo and Clarke, 2005; Lugo and Sharom, 2005). For many substrates, including those used in this study, passive permeability is a significant fraction of total transport and is quantitatively analyzed separately using the P-gp inhibitor, GF120918 (Evers et al, 2000; Acharya et al, 2008).

We measure the concentration of substrate in the apical chamber, denoted C_A, and the basolateral chamber, denoted C_B. However, the concentration of substrate in the cytosol, denoted C_C, and in the inner plasma membrane in contact with the P-gp binding site, denoted C_{PC}, cannot (yet) be measured rigorously in real time. These internal concentrations are variables of the mass action model and fitted by elementary rate constants for well-defined kinetic barriers, according to the measured values of C_B and C_A over time (Tran et al, 2005; Acharya et al, 2008).

We use the simplest competitive Michaelis-Menten mass action reaction to model P-gp transport:

$$T_0 + C_{PC} \underset{k_r}{\overset{k_1}{\rightleftarrows}} T_C \xrightarrow{k_2} T_0 + C_A \qquad (1)$$

$$T_0 + Q_{PC} \underset{k_{rQ}}{\overset{k_{1Q}}{\rightleftarrows}} T_Q \xrightarrow{k_{2Q}} T_0 + Q_A \qquad (2)$$

where T_0 is the empty transporter, C_{PC} is the substrate in the apical membrane inner monolayer, T_C is the transporter bound by substrate and C_A is the substrate after efflux into the apical chamber. For the inhibitor, labeled Q, Q_{PC} is the inhibitor in the apical membrane inner monolayer, T_Q is the transporter bound by inhibitor and Q_A is the inhibitor after efflux into the apical chamber. Loperamide and digoxin use additional transporters within the MDCKII cell line (Acharya et al, 2008). Both are used here as an inhibitors and the additional transporters are included in the fittings.

Table 1 shows the median consensus values of the elementary parameters used to fit the transport kinetics of amprenavir, digoxin, loperamide and quinidine (Acharya et al, 2006, 2008). Each parameter fitted gave good fits to all the data for up to 4-6 hours of transport. The values in Table 1 make considerable sense for P-gp function and structure (Tran et al, 2005; Acharya et al, 2006, 2008). For the MDCKII-hMDR1 cells, all drugs had essentially the same rate constant for association to P-gp, k_1, and essentially the same fitted membrane concentration of efflux active P-gp in the apical membrane, which was a benchmark for the validity of our mass action model and kinetic analysis (Tran et al, 2005; Acharya et al, 2006, 2008). We use the term "efflux active" to denote those P-gps whose effluxed substrate can reach the apical chamber, e.g. P-gps near the tips of the microvilli, as opposed to those P-gps near the base of the microvilli, whose effluxed substrate is nearly always reabsorbed back into the membrane before reaching the apical chamber (Acharya et al., 2006).

In our simulations, the value for k_1 was fixed at the value shown as it depends upon lipid lateral diffusion coefficient and the size to the entry way into the P-gp binding site (Tran et al, 2005). We expect k_1 to be roughly cell and tissue independent because it depends mostly on lipid lateral diffusion in the inner plasma membrane, although this has not yet been proven. In contrast, the

value of the membrane concentration of efflux active P-gp can be changed in the simulations, as this parameter can differ between cultured cells (Tang et al, 2002; Polli et al, 2001) and between tissues (Choo et al, 2006; Kurnik et al., 2008)).

This leaves three other significant parameters characterizing substrate and inhibitor interactions with the confluent cell monolayer and P-gp, all of which are probe-substrate parameters:

1) k_2, the efflux rate constant of the substrate from P-gp into the apical chamber.

2) k_r, the dissociation rate constant of the substrate from P-gp back into the inner apical membrane. The binding constant of the substrate to P-gp from the inner monolayer of the apical membrane is defined by the ratio of the fitted rate constants, i.e. $K_C=k_1/k_r$. Since k_1 is fixed at the consensus value (Table 1) here, k_r determines the binding constant.

3) K_{PC}, the partition coefficient of the substrate between the inner monolayer of the apical membrane and the cytosol. The product of $K_{PC}K_C$ is the binding constant to P-gp relative to the cytosolic concentration of substrate, so that the dissociation constant of the substrate to P-gp, relative to the cytosol, is $K_D =1/(K_{PC}K_C)$. When the drug is used as an inhibitor, $K_I = K_D$ to keep identities straight.

The two other partition coefficients, K_{BO}, between the basolateral chamber and the outer basolateral membrane monolayer and, K_{AO}, between the apical chamber and the outer apical membrane monolayer, see Fig. (1), have also been estimated independently (Tran et al, 2005) and the values in Table 1 are used in the simulations.

Results

Candidate IC50 Functions for Estimating K_I. The "standard" literature function, denoted SF, used to define an IC50 at some particular incubation time is (Gao et al, 2001; Zong and Pollack, 2003; Rautio et al, 2006):

$$\mathrm{SF}(\langle \mathrm{Q} \rangle) = \frac{\mathrm{nmol}(\mathrm{GF120918}) - \mathrm{nmol}(\langle \mathrm{Q} \rangle)}{\mathrm{nmol}(\mathrm{GF120918}) - \mathrm{nmol}(\langle \mathrm{Q} \rangle = 0)} \tag{3}$$

with <Q> being the inhibitor concentration added to both compartments. nmol(<Q>) , nmol(GF120918) and nmol(<Q>=0) refer to the nmol substrate transported in the presence <Q> in both chambers, in the presence of the potent P-gp inhibitor GF120918, and in the absence of inhibitor, respectively. If the data is without error, SF(<Q>) varies between 1 and 0. The inhibitor concentration required to reduce substrate transport by 50% is the IC50. Throughout this manuscript, the IC50 calculated by Eq. (3) will be called the SF50, in order to keep straight which candidate function is being tested. This candidate function can be used for B>A and A>B transport.

Other IC50 candidate functions were tested as well, see Balimane et al. (2008) for a current list of published candidate functions. Kalvass and Pollack (2007) proposed the following candidate function to replace the standard function of Eq. (3) for A>B transport only,

$$\mathrm{KP}(\langle \mathrm{Q} \rangle) = \frac{\mathrm{nmol}(\langle \mathrm{Q} \rangle = 0)}{\mathrm{nmol}(\langle \mathrm{Q} \rangle)} \left(\frac{\mathrm{nmol}(\mathrm{GF120918}) - \mathrm{nmol}(\langle \mathrm{Q} \rangle)}{\mathrm{nmol}(\mathrm{GF120918}) - \mathrm{nmol}(\langle \mathrm{Q} \rangle = 0)} \right) \tag{4}$$

Eq. (4) is identical to Kalvass and Pollock's Eqs. (12.1) and (12.4), but translated into our notation. We denote the IC50 obtained from Eq. (4) as the KP50.

Another candidate function used to calculate an IC50 is the efflux ratio:

$$\mathrm{ER}(\langle \mathrm{Q} \rangle) = \left(\frac{\mathrm{B} > \mathrm{A}\ \mathrm{nmol}(\langle \mathrm{Q} \rangle)}{\mathrm{A} > \mathrm{B}\ \mathrm{nmol}(\langle \mathrm{Q} \rangle)} \right) \Big/ \left(\frac{\mathrm{B} > \mathrm{A}\ \mathrm{nmol}(\langle \mathrm{Q} \rangle = 0)}{\mathrm{A} > \mathrm{B}\ \mathrm{nmol}(\langle \mathrm{Q} \rangle = 0)} \right) \tag{5}$$

ER50 denotes the IC50 from Eq. (5). This is a very good numerical approximation to the equation currently recommended in the FDA Guidance on Drug Interactions for measuring the IC50 for Pgp (Balimane et al., 2008), and it is simpler.

We also tested the simplest plausible candidate functions, i.e. just the A>B transport versus inhibition, termed absorption inhibition (AI) and the B>A transport versus inhibition termed secretion inhibition (SI),

$$\mathrm{AI}(\langle \mathrm{Q} \rangle) = \left(\frac{\mathrm{A} > \mathrm{B}\ \mathrm{nmol}(\langle \mathrm{Q} \rangle = 0)}{\mathrm{A} > \mathrm{B}\ \mathrm{nmol}(\langle \mathrm{Q} \rangle)} \right) \tag{6}$$

$$\mathrm{SI}(\langle \mathrm{Q} \rangle) = \left(\frac{\mathrm{B} > \mathrm{A}\ \mathrm{nmol}(\langle \mathrm{Q} \rangle)}{\mathrm{B} > \mathrm{A}\ \mathrm{nmol}(\langle \mathrm{Q} \rangle = 0)} \right) \tag{7}$$

AI50 denotes the IC50 from Eq. (6). SI50 denotes the IC50 from Eq. (7).

Experimental IC50 Curves. The error bars in Figs. (2 and 3) are standard deviations calculated using the equations derived in Appendix A in Supplementary Data. These are the appropriate equations to use for functions with products and quotients of variables with error, i.e. the candidate functions (Taylor, 1997). In all cases, our original triplicate data for nmol transported had <10% standard deviation.

Figure 2 shows the inhibition of 3uM quinidine (QND) A>B transport across the MDCKII-hMDR1 confluent cell monolayer by different P-gp competitive inhibitors/substrates. We chose QND as the probe-substrate because P-gp is it's only kinetically relevant transporter in the MDCKII-hMDR1 cell line, like amprenavir (Acharya et al., 2008). Fig. (2A) shows amprenavir (AMP) as inhibitor. The fitted K_I for amprenavir is shown by the arrow at ~5uM. Clearly, the KP50~10uM from Eq.(4) makes a better estimate of K_I than the SF50~30-40uM from Eq.(3) or the AI50~20uM from Eq.(6). The inhibition curves have the shape of the 1-site competitive inhibition curve demarked HH, for Henderson-Hasselbach, reasonably well.

Fig. (2B) shows loperamide (LPM) as inhibitor. The KP50~0.4uM from Eq.(4) makes a better estimate of the fitted $K_I \cong 0.1$uM than the SF50~1-2uM from Eq.(3) or the AI50~1uM from Eq.(6). There is also a "bounce" in the KP curve starting at a concentration about an order of magnitude below the K_I. This experiment has been done 3 times with basically the same result: the fraction transported goes down to 0.8-0.9 around 0.01uM LPM and rises to about 1.1 around 0.01-0.05uM LPM. For all 3 experiments the KP50 is in the range 0.3-0.5.

This "bounce" became less variable in magnitude when the cells are preincubated with the inhibitor for an hour and the measurement was made 2 hours later, as we have done here. Shorter preincubation times (0.5 hr) or longer measurement times (4hrs) typically yielded greater variability. Our simplest hypothesis is it involves changes in microvilli morphology, e.g. longer or shorter, which can strongly alter passive and active efflux via drug re-absorption by microvilli (Tran et al, 2005; Acharya et al, 2006, 2008).

Fig. (2C) shows quinidine (QND) itself as the inhibitor, i.e. excess cold quinidine was added. The KP50~1-2uM from Eq.(4) makes a better estimate of the $K_I \cong 0.1$uM than the SF50~4-5uM from Eq.(3) or the AI50~3uM from Eq.(6). So, for all three cases in Fig. (2), the Kalvass and Pollock (2007) KP50 was closer to the K_I.

Figure 3 shows the inhibition of digoxin (DGX) transport in both directions. Fig. (3A&B) shows 0.03 uM digoxin transport inhibited by quinidine in the A>B and B>A directions respectively. The fitted K_I values are shown by the arrow and the dotted line represents the 50% inhibition of P-gp activity. Fig. (3C&D) shows 0.1 uM digoxin transport inhibited by verapamil (VRP) in the A>B and B>A directions respectively. The ER candidate function, Eq. (5), is closer to the K_I for quinidine, but there is not much difference between the candidate functions. The K_I for verapamil has not been fitted yet.

Simulations. We have observed that the IC50 measured for a number of inhibitors using several commonly used candidate functions overestimate the K_I by 2-100 fold, depending upon the probe substrate and the inhibitor. The mass action kinetic model was analyzed to determine what causes $IC50/K_I > 1$.

The first step is to determine whether simulations show the same overestimate for $IC50/K_I$, which might not be expected since the model fitted the K_I in the first place. **Figure 4** shows the simulation of the nmol transported over time for 2uM of a quinidine-like probe-substrate in both directions as a function of concentration for a quinidine-like inhibitor whose K_I=0.1 uM. Complete inhibition of P-gp is shown by the thick black line, denoted GF120918 here, in the middle and yields the passive permeability of the probe-substrate through the bilayer, since there is no transporter for quinidine in the mass action model. Below the GF120918 line is the A>B

transport and above the GF120918 line is the B>A transport, as a function of inhibitor concentration (0.3 and 1 uM respectively). The dashed lines at top and bottom show inhibitor-free transport in both directions, i.e. when <Q>=0, and P-gp efflux is fully functioning (e.g., B>A rate is larger than the A<B rate). According to Eq. (3), the SF50 in either direction would be halfway between the dashed line (without inhibitor, 0 uM) and the black solid line (for completely inhibited P-gp; GF120918).

The simulated SF50 is shown by the large black dots at different time points and is about 0.7uM, i.e. **a** 7-fold larger than the K_I used to calculate these simulations in the first place. The simulated nmol transported starting with either 0.1 or 5uM probe-substrate gave essentially the same results (not shown), proving that the difference between SF50 and K_I is not due to probe-substrate concentration. Likewise, since there were no transporters in this simulation, aside from P-gp, the overestimate cannot be due to another transporter. It is due to the IC50 candidate function.

The IC50/ K_I Overestimation Equation. Since our data and the mass action kinetic model predict that the IC50 will overestimate the inhibitor's K_I, we can use simulations to understand why. **Figure 5** shows the simulated concentrations of a 2uM quinidine-like probe-substrate over time. Fig. (5A) shows for B>A transport, the concentration in the basolateral chamber, C_B, starts at 2uM and decreases continuously, while the concentration in the apical chamber, C_A, increases continuously to above 3uM, which exceeds the initial concentration in the donor chamber because the volume of the basolateral chamber is 3-fold greater than that of the apical chamber. The cytosolic concentration, C_C, rises slowly and converges with C_B at steady-state. After 6 hrs, the system has reached its true steady-state, where the flux from the apical chamber by passive permeability into the cytosol equals the ATP driven active transport by P-gp into the apical chamber, plus the passive permeation from the cytosol to the apical chamber.

The usual assumption of an IC50 experiment is that there is a steady-state period, wherein the rate of product formation is approximately constant over some period of time. For B>A transport, there is no clear steady-state for C_A until the true steady-state, which occurs sometime after 6 hours (Fig. 5A). Note that the "jump" of the concentration in the cytosol, C_C, at the first time point in the simulation (6 minutes), is not a computational artifact. This is the first time point taken in our experiments (Tran et al, 2004, 2005; Acharya et al, 2006). This jump is due only to connecting a straight line between t=0 and t=6min and would become smooth if we had plotted earlier time points from the simulation.

Fig. (5B) shows for A>B transport that there is a striking difference in the shapes of the concentration curves. The concentration in the apical chamber, C_A, starts at 2uM, decreases slowly and reaches a true steady-state around 1.5 uM. The concentration in the cytosol, C_C, jumps rapidly to about 0.16 uM, a quasi steady-state, and then decreases slightly over time to the true steady-state of about 0.13 uM. We use quasi steady-state to denote a relatively flat concentration curve in the cytoplasm that eventually reaches the true steady-state. The term cannot defined rigorously because there is a continuum of more or less relatively flat concentration curves observed in these simulations. However, the quasi steady-state in conjunction with the mass action kinetic equations can be used to provide guidance for understanding the overestimate of K_I by the IC50's of the candidate functions.

The conditions met during the quasi steady-state for A>B transport is that the cytosolic C_C is essentially constant over time, yielding a time independent IC50, and that $C_C << C_A$. We use these conditions on the mass action kinetic model of P-gp mediated transport through a confluent cell monolayer to derive an approximate solution for $SF50/K_I$, which is shown in Appendix B in Supplementary Data. This equation is

$$\frac{SF50}{K_I} = \frac{[Pgp]K_C K_{PC} k_2}{\left(\frac{4}{d}P_{BC} + 2k_B + \frac{4}{d}P_{AC} + 2k_A\right)} \quad (8)$$

All terms on the right hand side, both numerator and denominator, are for the probe substrate and are defined in Table 1 using the same units. The numerator shows all of the parameters which control P-gp mediated efflux from the cells, including the membrane concentration of efflux active P-gp, denoted [P-gp]. Increasing the numerator leads to a greater overestimate. The denominator shows all of the parameters that control influx into the cells, i.e. the +GF120918 lipid bilayer/tight junction permeation, denoted P_{BC} and P_{AC}, and the transport by other transporters, denoted k_B and k_A. The bilayer thickness is denoted d, in the units of nm, and we use d=4nm for our simulations, i.e. $4/d=1nm^{-1}$. Thus, all of these terms have the units of s^{-1}. Increasing the denominator leads to a smaller overestimate. The value of $SF50/K_I$ is always greater than 1 when the approximations used in the derivation are valid. Eq. (8) is the molecular expression of the schematic proposed in Litman et al. (2003).

Using simulations, we assessed the accuracy of Eq. (8). Changing each parameter ten-fold, up or down, produced appropriate 7-12 fold changes in the predicted values of $SF50/K_I$, data not shown. The decrease in $SF50/K_I$ as the passive permeability coefficients of the probe substrates increase is well predicted by Eq. (8), $R^2>0.95$, for both A>B and B>A transport. This shows that the direction of transport does not matter for Eq. (8), despite the differences in the shapes of the kinetic curves. Thus, the quasi steady-state condition for A>B transport was not necessary to derive Eq. (8), but it was sufficient. This directional independence is not shared by all other

membrane specific candidate functions for IC50 calculations, e.g. the Kalvass and Pollack (2007) equation in the B>A direction, appropriately transformed, has a very different IC50 than that for A>B transport.

Experimental validation of Eq. (8) is examined in Table 2, wherein the measured SF50s in this work are "corrected" by Eq. (8) and compared with the K_I values shown in Table 1. The kinetically fitted K_I and the K_I estimated using Eq. (8) are in good agreement, except for the case of digoxin as the probe-substrate and quinidine as the inhibitor. Since the simulations showed no obvious discrepancy, it appears that there remain other unknown factor(s) in the IC50 experiment. Further work involving a broader database will be required to understand these factors.

What is the relationship between a K_I, an IC50 and the fraction of P-gp bound by the substrate? **Figure 6** shows a simulation of the inhibition of 0.03uM digoxin-like A>B transport by quinidine-like inhibitor using the Standard Function, Eq. (3), the Kalvass and Pollack equation, Eq. (4), and the decrease in the fraction of P-gp bound by the digoxin-like probe-substrate relative to that bound without inhibitor. Interestingly, the fraction of P-gp bound by digoxin is nearly identical to the inhibition curve of the Standard Equation. The KP50~2uM underestimates the concentration of 50% reduction in digoxin binding to P-gp, ~4uM.

Compared with the experimental data of the same case, Fig. (3A&B), the simulation shows a greater separation between KP50 and SF50 than the experimental data. For the data, KP50~6uM and SF50~10uM. The larger IC50 values for the experiments may be due to the "bounce" seen in Figs. (2B&C) or it may suggest that digoxin and quinidine don't compete as well as the other

pairs tested. The simulations assume pure competitive binding using fitted binding constants obtained using drugs alone.

The Physical Mechanism for the Overestimate Equation. The physical mechanism for the overestimate of SF50 compared to K_I is explained by the basic shape of a single-site competitive binding curve. We can vary any of the kinetic parameters in Eq. (8) to show this and have chosen to use the P-gp concentration in the membrane. **Figure 7** is a simulation of the concentration of P-gp bound to the digoxin-like probe substrate as a function of concentration of a quinidine-like inhibitor. There is 0.03uM of a digoxin-like probe-substrate and the elementary parameters from Table 1 were used in the simulations. The solid line is for 200uM as the membrane concentration of efflux active P-gp, as in Table 1. Without inhibitor, about 0.12uM of P-gp is bound by substrate after a 2-hr incubation. To reduce the substrate-bound P-gp by 50% required about 0.7uM inhibitor. This simulates the data in Fig. (3A&B). On the other hand, the dotted line simulation has half the membrane concentration of efflux active P-gp, 100uM, and the inhibitor free concentration of digoxin-bound P-gp was 0.1uM. To reduce this value by 50% requires about 1.2uM inhibitor. A one-site competitive binding curve flattens out as the fraction bound decreases and more inhibitor is required to reduce the substrate-bound P-gp by 50%. In both cases, K_I=0.1uM is the same and so the overestimate is 7-fold and 12-fold, respectively.

Inside-Out Vesicles. Because of the difficulty in getting the confluent cell monolayer system to yield a K_I simply, simulations of inside-out plasma membrane vesicles (Glavinas et al., 2008) were undertaken. These vesicles have been proposed as a simpler system for fitting a K_I or a Michaelis constant Km, depending on the experiment, because the binding site is directly exposed to the incubation medium. The drug would partition into the membrane, but there is no known permeability barrier from that membrane monolayer to the P-gp binding site, unlike the

drug flip-flop across the plasma membrane that is required when the drug binds to the outer basolateral monolayer.

Starting from the appropriate mass action kinetic reactions, shown in Appendix C in Supplementary Data, we calculated that the small volume of the vesicles, 1-10um diameter, would allow the true steady-state to be achieved within seconds, see Eq. (D2) in Appendix D in Supplementary Data. This allowed approximations that yielded the following equation,

$$\frac{SF50}{K_I} \cong 1 + K_{PC} K_C C_O(0) \tag{9}$$

i.e., Pgp in inside-out vesicles should behave like a soluble enzyme (Cheng and Prusoff, 1973). It is important to note that these simulations assumed that the vesicle were unilamellar and that the larger concentration of probe-substrate and inhibitor within the vesicle due to P-gp had no impact on the P-gp binding site within the outside monolayer of the vesicle. These assumptions remain to be tested by experiment.

Discussion

An inhibitor's K_I or IC50 are the two basic ways of rank ordering inhibitors with respect to their activity against an enzyme or transporter. But they measure two quite different physicochemical properties. The $K_I=1/(K_{QPC}K_Q)$ is the dissociation constant for the inhibitor from P-gp to the cytosol, i.e. the inverse of product of the binding constant of the inhibitor from the bilayer to P-gp, K_Q, and the partition coefficient of the inhibitor into the bilayer from the cytosol, K_{QPC}. This is an equilibrium thermodynamic parameter defined by the sum of two equilibrium thermodynamic free energies. The IC50 is the concentration of inhibitor required to reduce the transport of the probe-substrate by 50% from a chosen probe-substrate concentration and at a chosen incubation time. This is a profoundly kinetic parameter that depend upon the K_I and the kinetic parameters required to model the evolution of the system. Here, we have discovered which kinetic parameters make this definition.

Previously, we showed that the measured IC50 was much greater than the fitted K_I for P-gp to amprenavir, loperamide, and quinidine (Acharya et al, 2006). Starting from the standard literature equation for the SF50, Eq. (3), we have derived a very simple approximate equation that defines the ratio of $SF50/K_I$, Eq. (8), shown in Appendix A of the Supplemental Data. The $SF50/K_I$ ratio increases as the parameters driving substrate efflux increase, e.g. membrane concentration of efflux active P-gp, substrate binding constant, substrate partition coefficient and substrate efflux rate constant. Increases in these parameters reduce the cytosolic concentration of the substrate, the amount of substrate bound P-gp and increases the concentration of inhibitor needed to reduce the substrate bound P-gp by 50%, Fig. (7). Eq. (8) also predicts that the $SF50/K_I$ ratio decreases as the passive permeability increases, either by bilayer permeation or the

presence of other transporters. It is simply the math of a 1-site binding reaction with inhibition by competitive binding happening within a small volume.

If it were the case that the MDCKII_hMDR1 cell line had another active transporter in the apical membrane that shared P-gp's substrate range and was inhibited by GF120918, then the efflux active surface density of P-gp shown in Table 1 would be an average of the efflux active surface densities of P-gp and this other transporter, weighted by their respective kinetic parameters. While loperamide does use another transporter in the basolateral membrane of this cell line (Table 1, Acharya et al., 2008), our fits show that it is bidirectional, i.e. not an active transporter like MRP2 and BCRP. It appears that the MDCKII cell line shows no functional expression of MRP2 or BCRP (Lalloo et al, 2004; Wang et al, 2007; Weiss et al 2007; Solazzo et al, 2009).

Eq. (8) can be used to correct the SF50 and yield a good estimate for the K_I in most cases, Table 2. The exception was digoxin inhibited by quinidine, where the correction reduced the overestimate from about 90-fold to about 20-fold, which is still a large overestimate. Taub et al. (2005) found several P-gp substrates that did not inhibit other P-gp substrates very well and noted that P-gp can bind more than one substrate (Littman et al., 1997; Shapiro and Ling, 1997; Allers et al., 2009). One hypothesis is that digoxin binds predominantly to one site and quinidine binds predominantly to the other site, yielding weaker inhibition compared with drugs that bind predominantly to the same site. If so, then the two sites have cooperativity. We are unaware of any study showing that both substrates are transported from the same P-gp simultaneously or synchronously.

A second hypothesis starts with the finding that digoxin transport across the confluent MDCKII-hMDR1 cell monolayer requires one or more transporters other than P-gp, in both the apical and

basolateral membranes, Table 1 (Acharya et al., 2008). Our analysis of quinidine transport showed that only P-gp is required for its transport (Acharya et al., 2008). However, that does not mean that quinidine cannot interact with these other transporters, it is just that the transporters do not provide a kinetically significant transport pathway for quinidine, whose bilayer permeability is much larger than digoxin's, Table 1. This hypothesis is consistent with the idea that there are two binding sites for these drugs, but one is on P-gp and the other is on the other digoxin transporter.

Using standard steady-state Michaelis-Menten equations, Kalvass and Pollack (2007) predicted that the standard equation, Eq. (3), would overestimate the K_I. Our experiments showed that the KP50 and the ER50 values were usually closer to the K_I than the IC50 values for the other candidate functions. However, none of the candidate function's IC50 values estimated the K_I that well, Figs. (2 and 3). Interestingly, when the analysis given to the SF candidate function, Eq. (3), to derive the overestimation equation, Eq. (8), in Appendix A of Supplemental Data was performed on the KP candidate function, the result was $KP50/K_I=1$, not shown, even though the Figs. (2 and 3) show that was not the case.

The correction factor given by Eq. (8) has no effect on the rank order of P-gp inhibitors when using a single probe-substrate with the same in vitro cell line, since it would be the same correction for all inhibitors. Changing the probe-substrate with the same in vitro cell line would change the IC50 values, but would not affect the rank order.

What is not clear is whether inhibitor rank order would be maintained from one in vitro cell line to another in vitro cell line or when extrapolated in vivo. Recall for the P-gp substrate used as a competitive inhibitor that $K_I=1/(K_{QPC}*K_Q)$. If the binding constant of the inhibitor, K_Q, were

about the same between two cell types, which not known but is a reasonable speculation insofar as the acyl chains in plasma membranes are similar, then their rank ordering would depend largely upon their relative partition coefficients to the inner apical membrane, K_{QPC}. Whichever drug had the larger partition coefficient would have the smaller K_I and possibly a smaller IC50. We found quite a lot of sensitivity of partition coefficients between the drugs, Table 1 (Tran et al, 2005). In a different cell line or in vivo, it would be very hard to predict whether the partition coefficients would remain in the same rank order. More measurements of the partition coefficients as a function of liposome composition would clarify this part of the extrapolation problem.

Eq. (8) has an immediate application to the in vivo experiments. Choo et al. (2006) found that the tariquidar dose in mice needed to increase the tissue penetration of ^{11}C-N-desmethyl-loperamide to 50% of complete inhibition of Pgp was much higher for the brain than for the testes. They gave several speculations to explain this, including that perhaps there was a higher Pgp surface density in the blood brain barrier, following the analysis in Litman et al. (2003). Kurnik et al. (2008) found in humans that tariquidar could fully inhibit Pgp in lymphocytes, but not in the blood brain barrier.

Eq. (8) gives us a testable hypothesis to explain these findings. If the ratio of membrane concentration of efflux active P-gp to probe-substrate passive permeability coefficients across the apical membrane is greater in the brain than in the testes and the lymphocytes, which seems reasonable, then Eq. (8) can explain these observations and allow us to estimate other essential kinetic parameters. If the ratios are opposite, then a very different mechanism than commonly believed must dominate the kinetics of P-gp mediated transport in these organs.

Eq. (8) can also clarify another in vivo issue. Kannan et al. (2009) used an analysis in Kalvass and Pollack (2007) to speculate that the difference between the KP50, identified by them as the K_I of the inhibitor, and the SF50, implied that over 80% of the P-gp in the blood brain barrier must be bound to achieve 50% inhibition of transport into the brain. They proposed that there could be "spare transporters" in the blood brain barrier to account for this effect. We see from Eq. (8) that the overestimate cited can be explained by our model, without invoking "spare transporters". The Kalvass and Pollack (2007) candidate function does not equal the K_I for the drugs we have tested and the SF candidate function predicts the fraction of substrate bound P-gp quite well, Fig. (6).

In summary, we have found that all of the IC50 candidate functions tested in this work overestimate the K_I. The $SF50/K_I$ overestimate depends on the membrane concentration of efflux active P-gp in the apical membrane and the probe-substrate kinetic parameters, Eq. (8). This equation can be used to refine the estimate for the K_I, Table 2. Thus, our kinetic model yields a simple and accurate equation that can serve as a tool for *in vitro-in vivo* extrapolation.

References

Acharya P, Tran TT, Polli JW, Ayrton A, Ellens H and Bentz J (2006) P-gp expressed in a confluent monolayer of MDCKII- hMDR1 cells has more than one efflux pathway with cooperative binding sites. *Biochemisty*, **45**:15505-15519.

Acharya P, Polli JW, Ayrton A, Ellens H and Bentz J (2008) Kinetic identification of membrane transporters that assist P-gp mediated transport of digoxin and loperamide through a confluent monolayer of MDCKII-hMDR1 cells. *Drug Metab. Dispos.* **36**:452-460.

Bartholome´ K, Rius M, Letschert K, Keller D, Timmer J, and Keppler D (2007) Data-based mathematical modeling of vectorial transport across double-transfected polarized cells. *Drug Metab Dispos* **35**:1476–1481.

Balimane PV, Marino A, Chong S (2008) P-gp Inhibition Potential in Cell-Based Models: Which "Calculation" Method is the Most Accurate? *AAPS J.* **10**:577-86.

Bentz J, Tran TT, Polli JW, Ayrton A and Ellens H (2005) The steady-state Michaelis-Menten analysis of P-glycoprotein mediated transport through a confluent cell monolayer cannot predict the correct Michaelis constant Km. *Pharm Res.* **22**:1667-1677.

Borst P, Zelcer N, van de Wetering K and Poolman B (2006) On the putative co-transport of drugs by multidrug resistance proteins. *FEBS Lett.* **580**:1085–1093.

Chang JH and Benet LZ (2005) Glucuronidation and the transport of the glucuronide metabolites in LLC-PK1 cells. *Mol Pharm.* **2**:428-34.

Cheng Y and Prusoff WH.(1973). Relationship between the inhibition constant (K_I) and the concentration of inhibitor which causes 50 per cent inhibition (IC50) of an enzymatic reaction. *Biochem. Pharmacol.* **22**:3099-3108.

Choo EF, Kurnik D, Muszkat M, Ohkubo T, Shay SD, Higginbotham JN, Glaeser H, Kim RB, Wood AJJ, and G. R. Wilkinson GR (2006). Differential in vivo sensitivity to inhibition of P-glycoprotein located in lymphocytes, testes, and the blood-brain barrier. *J. Pharmacol. Exp. Ther.* **317**:1012-1018.

Collett A, Tanianis-Hughes J, Carlson GL, Harwood MD and Warhurst G (2005) Comparison of P-glycoprotein-mediated drug–digoxin interactions in Caco-2 with human and rodent intestine: Relevance to in vivo prediction *Eur. J. Pharm. Sci.* **26**:386–393.

Endres CJ, Hsiao P, Chung FS and Unadkat JD (2006) The role of transporters in drug interactions. *Eur. J. Pharm. Sci*. **27**:501-517.

Evers R, Kool M, Smith AJ, van Deemter L, de Haas M and Borst P (2000) Inhibitory effect of the reversal agents V-104, GF120918 and Pluronic L61 on MDR1 P-gp, MRP1- and MRP2-mediated transport. *British J. Cancer*. **83**:366-374.

Gao J, Murase O, Schowen RL, Aube J and Borchardt RT (2001) A functional assay for quantitation of the apparent affinities of ligands of P-glycoprotein in Caco-2 cells. *Pharm. Res.* **18**:171-6.

Giri N, Agarwal S, Shaik N, Pan G, Chen Y and Elmquist WF (2009) Substrate-dependent breast cancer resistance protein (Bcrp1/Abcg2)-mediated interactions: consideration of multiple binding sites in in vitro assay design. *Drug Metab Dispos* **37**:560-70.

Glavinas H, Mehn D, Jani M, Oosterhuis B, Heredi-Szabo K and Krajcsi P (2008) Utilization of membrane vesicles to study drug-ABC transporter interactions. *Expert Opin. Drug Metab. Toxicol.* **4**:721-732.

Hah J S, Ryu JW, Lee W, Kim BS, Lachaal M, Spangler RA and Jung CY (2002). Transient changes in four GLUT4 compartments in rat adipocytes during the transition, insulin-stimulated to basal: Implications for the GLUT4 trafficking pathway. *Biochemistry* **41:**14364-14371.

Ho NFH, Raub TJ, Burton PS, Bausuhn CL, Adson A, Audus KL and Borchardt R (2000). Quantitative approaches to delineate passive transport mechanisms in cell culture monolayers. In: *Transport Processes in Pharmaceutical Systems*. Eds. GL Amidon and V Lee. Marcel Dekker, New York. pp. 219-316.

Kalvass JC and Pollack GM (2007) Kinetic considerations for the quantitative assessment of efflux activity and inhibition: implications for understanding and predicting the effects of efflux inhibition. *Pharm Res* **24**:265-76.

Kannan P, John C, Zoghbi SS, Halldin C, Gottesman MM, Innis RB and Hall MD (2009) Imaging the Function of P-Glycoprotein With Radiotracers: Pharmacokinetics and In Vivo Applications. *Clin. Pharmacol. Ther.* **86**:368-77

Kurnik D, Gbenga G, Sofowora, Donahue JP, Usha B Nair, Wilkinson GR, Wood AJJ and Mordechai M (2008) Tariquidar, a selective P-glycoprotein inhibitor, does not potentiate loperamide's opioid brain effects in humans despite full inhibition of lymphocyte P-glycoprotein. *Anesthesiology* **109**: 1092–1099.

Lalloo AK, Luo FR, Guo A, Paranjpe PV, Lee SH, Vyas V and Rubin E, Sinko PJ (2004) Membrane transport of camptothecin: facilitation by human P-glycoprotein (ABCB1) and multidrug resistance protein 2 (ABCC2). *BMC Med.* 2:16.

Litman, T, Skovsgaard T and Stein WD (2003). Pumping of drugs by P-glycoprotein: A two-step process? *J. Pharmacol. Exp. Ther.* **307**:846-853.

Litman T, Zeuthen T, Skovsgaard T, and Stein WD (1997) Competitive, non-competitive and cooperative interactions between substrates of P-glycoprotein as measured by its ATPase activity. *Biochim Biophys Acta* **61:**169 –176.

Loo TW and Clarke DM (2005) Recent Progress in Understanding the Mechanism of P-Glycoprotein-mediated Drug Efflux. *J. Membr. Biol.* **206**:173-185.

Lugo MR and Sharom FJ (2005) Interaction of LDS-751 with P-glycoprotein and mapping of the location of the R drug binding site. *Biochemistry* **44**:643-55.

Nies AT, Schwab M and Keppler D (2008) Interplay of conjugating enzymes with OATP uptake transporters and ABCC/MRP efflux pumps in the elimination of drugs. *Expert Opin. Drug Metab. Toxicol.* **4**:545-568.

Polli, JW, Wring SA, Humphreys JE, Huang L, Morgan JB, Webster LO and Serabjit-Singh CJ (2001) Rational use of in vitro P-glycoprotein assays in drug discovery. *J. Pharm. Exp. Therap.* **299**:620-628.

Rautio J, Humphreys JE, Webster LO, Balakrishnan A, Keogh JP, Kunta JR, Serabjit-Singh CJ and Polli JW (2006) In Vitro P-glycoprotein Inhibition Assays for Assessment of Clinical Drug Interaction Potential of New Drug Candidates: A Recommendation for probe-substrates. *Drug Metab Dispos.* **34**:786-792.

Shapiro AB and Ling V (1997) Positively cooperative sites for drug transport by P-glycoprotein with distinct drug specificities. *Eur J Biochem* **250:**130 –137.

Shitara Y, Horiea T and Sugiyama Y (2006) Transporters as a determinant of drug clearance and tissue distribution. *Eur. J. Pharm. Sci.* **27**:425–446.

Solazzo M, Fantappiè O, D'Amico M, Sassoli C, Tani A, Cipriani G, Bogani C, Formigli L and Mazzanti R (2009) Mitochondrial expression and functional activity of breast cancer resistance protein in different multiple drug-resistant cell lines. *Cancer Res.* **69**:7235-42.

Sun H and Pang KS (2008) Permeability, Transport, and Metabolism of Solutes in Caco-2 Cell Monolayers: A Theoretical Study. *Drug Metab Dispos* **36**:102-123.

Tang F, Horie K and Borchardt RT (2002) Are MDCK cells transfected with the human MDR1 gene a good model of the human intestinal mucosa? *Pharm Res*. **19**: 773-779.

Taub ME, Podila L, Ely D and Almeida I (2005). Functional assessment of multiple P-glycoprotein probe substrates: Influence of cell line and modulator concentration on P-gp activity. *Drug Metab Dispos.* **33**:1679-1687.

Taylor JR (1997). An Introduction to Error Analysis: The Study of Uncertanties in Physical Measurements. University Science Books. 2nd Edition. Chapter 3.

Tran TT, Mittal A, Gales T, Maleeff B, Aldinger T, Polli JW, Ayrton A, Ellens H and Bentz J (2004) An Exact Kinetic Analysis of Passive Transport across a Polarized Confluent MDCK Cell Monolayer Modeled as a Single Barrier. *J. Pharm. Sci*. **93**:2108-2123.

Tran TT, Mittal A, Aldinger T, Polli JW, Ayrton A, Ellens H and Bentz J (2005) The elementary mass action rate constants of P-gp transport for a confluent monolayer of MDCKII-hMDR1 cells. *Biophys. J.* **88**:715-738.

Wang Q, Strab R, Kardos P, Ferguson C, Li J, Owen A and Hidalgo IJ (2008) Application and limitation of inhibitors in drug-transporter interactions studies. *Int J Pharm.* **356**:12-8.

Weiss J, Rose J, Storch CH, Ketabi-Kiyanvash N, Sauer A, Haefeli WE and Efferth T (2007) Modulation of human BCRP (ABCG2) activity by anti-HIV drugs. *J Antimicrob Chemother.* **59**:238-45.

Zong J and Pollack GM (2003) Modulation of P-glycoprotein transport activity in the mouse blood-brain barrier by rifampin. *J. Pharmacol. Exp. Ther.* **306**:556-562.

Footnotes

[#]These authors contributed equally to this work.

[&] Present Address: Department of Cellular and Molecular Pharmacology, UCSF, Mission Bay Campus, San Francisco, CA, USA 94158-2517

Figure Legends

Figure 1. Model of a confluent cell monolayer, with the apical membrane on top and the basolateral membrane below, where it binds to the polycarbonate insert. Passive permeability occurs in both directions. P-gp expressed on the apical membrane transports substrate from the inner apical membrane monolayer into the apical chamber. The concentration of substrate in the apical and basolateral chambers, C_A and C_B, are measured, while the concentration of substrate in the inner plasma membrane, C_{PC}, and the cytosol, C_C, are predicted as part of the mass action modeling and data fitting process. For some compounds, such as digoxin and loperamide there are other transporters expressed by the MDCKII-hMDR1 confluent cell monolayer.

Figure 2. Inhibition of 3uM quinidine A>B transport across the MDCKII-hMDR1 confluent cell monolayer by different P-gp competitive inhibitors/substrates: amprenavir (2A) loperamide (2B) and quinidine (2C). The smooth thick broken line, denoted HH, is the predicted 1-site binding curve using the fitted K_I of the inhibitor, i.e. shown where it crosses the dotted line at 50%. The Standard inhibition curve from Eq(3) is shown with open squares (□); Kalvass and Pollock curve from Eq. (4) shown by the open triangles (△). The curve shown by open circles (O) is for the AI equation, Eq. (6). Data points show the mean +/- standard deviation (n=3). The error bars are standard deviations, calculated using Eqs. (C.9), (C.12) and (C.15) in Appendix C in Supplementary Data, which are the appropriate equations to use for functions which are ratios of variables with error, i.e. the candidate functions (Taylor, 1997).

Figure 3 Digoxin A>B and B>A transport across the MDCKII-hMDR1 confluent monolayers in the presence of inhibitors/substrates. 0.03uM digoxin inhibited by quinidine, where Fig. (3A) is A>B and Fig. (3B) is B>A. 0.1uM digoxin inhibited by verapamil, where Fig. (3C) is A>B and Fig. (3D) is B>A. For A>B transport, Std inhibition curve from Eq. (3) is shown with open

squares(□); Kalvass and Pollock curve from Eq. (4) shown by the open triangles(△); Efflux Ratio curve from equation Eq. (5) is shown by the closed diamonds (♦); and Absorption Inhibition curve from equation Eq. (6) is shown by open circles (O). For B>A transport, Std inhibition curve from Eq. (3) is shown with open squares(□); Efflux Ratio curve from equation Eq. (5) is shown by the closed diamonds (♦); and Secretory Inhibition curve from equation Eq. (7) is shown by open circles (O). Data points show the mean +/- standard deviation (n=3).

Figure 4. Simulation of nmol transported over time for 2uM of an quinidine-like probe-substrate, denoted QND, in the presence of increasing concentrations of a quinidine-like inhibitor, i.e. with the same kinetic parameters as quinidine, including K_I=0.1uM. Complete inhibition of P-gp by GF120918 is simulated by the thick black line in the middle. B>A transport is shown by the thin lines above the GF120918 control, with the inhibitor concentration shown beside in uM units. A>B transport is shown by the thin lines below the GF120918 control, with the inhibitor concentration shown beside in uM units. Clearly, the IC50 is in the range of 0.7 uM, in both directions, i.e. about 7 times larger than the K_I.

Figure 5. Simulations of the concentrations over time of a quinidine-like probe-substrate, i.e. using the quinidine kinetic parameters shown in Table 1, in the basolateral, cytosol and apical compartments, starting with 2uM in the donor compartment. (A) shows the case when the donor is the basolateral chamber, i.e. B>A. No steady-state is established prior to the true steady-state which will occur when C_C=C_B . The concentration in the apical chamber will reach somewhat less than 4 uM, since the apical chamber is 0.5 mL and the basolateral chamber is 1.5 mL. (B) shows the case when the donor is the apical chamber, i.e. A>B. A quasi steady-state is

established within minutes in the cytosol, C_C~0.2 uM, which slowly decreases slightly to the true steady-state, which will occur when $C_C=C_B$.

Figure 6. A simulation of inhibition of 0.03uM digoxin A>B transport by quinidine as measured by the KP and SF candidate functions, Eqs. (3 and 4), and by the fraction of digoxin -bound P-gp relative to the digoxin-bound P-gp bound without inhibitor. The K_I for quinidine is shown, which is more than 10-fold smaller than the KP50, SF50 and the mark for 50% P-gp bound by digoxin. The fraction bound is nearly identical to the SF candidate function.

Figure 7. The concentration of substrate-bound P-gp as a function of inhibitor concentration for A>B transport. The solid line shows the case for 0.03uM of a digoxin-like probe-substrate inhibited by a quinidine-like inhibitor, using the parameters from Table 1. To reduce the substrate-bound P-gp from about 0.12uM to 0.6uM required about 3uM of inhibitor. When initial concentration of efflux active P-gp is halved to 100uM, then the inhibitor-free value of substrate-bound P-gp is decreased to about 0.10uM. To reduce the substrate-bound P-gp by 50%, to 0.05uM, required about 0.7uM of inhibitor, i.e. nearly half as much inhibitor, as was predicted by Eq. (8).

Table 1. Fitted Parameter Values for MDCKII-hMDR1 confluent cell monolayers.

Substrate	Association to P-gp k_1 ($M^{-1}s^{-1}$) [a]	Membrane Concentration of Efflux Active P-gp [P-gp] (uM) [b]	Efflux to Apical Chamber k_2 (s^{-1}) [c]	Partition Coefficients [d]			Binding Constant to P-gp from Inner Apical Membrane K_C (M^{-1}) [e]	Dissociation Constant to P-gp from cytosol K_D (uM) [f]	Passive Permeability Coefficient at true steady-state [g] P_{BC} P_{AC} (nm/sec) Other Transporters k_B k_A (s^{-1})	
				K_{PC}	K_{AO}	K_{BO}				
Amprenavir	$2x10^{+9}$	200	150	200	150	200	1,000	5	400 0	400 0
Digoxin	$2x10^{+9}$	200	10	ND [h]	ND [h]	ND [h]	ND [h]	3 [h]	30 30	30 2
Loperamide	$2x10^{+9}$	200	2	3,000	700	1000	4,000	0.1	350 100	350 0
Quinidine	$2x10^{+9}$	200	5	700	70	100	15,000	0.1	500 0	500 0

Legend for Table 1.

[a] All values are from Acharya et all (2008). These are median values obtained for the association rate constant fits. This is the rate constant from flip-flop across the basolateral membrane to association with the P-gp binding site

Table 1 cont'd.

[b] Median values for the membrane concentration of efflux active P-gp in the apical membrane inner monolayer for each of the three drugs. The units are per liter of membrane, which can be converted to P-gp/um^2 by multiplying by 0.8. This number may be 10-20 times smaller than the actual surface density since only substrate released at the tips of the microvilli are likely to reach the apical chamber, rather than being absorbed back into the microvilli membrane and starting over.

[c] Median value for the efflux rate constant k_2.

[d] The partition coefficient between the cytosol and the inner plasma/apical monolayer, K_{PC}, between the apical outer monolayer and the apical chamber, K_{AO}, and between the bsolateral outer monolayer and the basolateral chamber, K_{BO}, are shown. Partition coefficients were estimated using 0.1um extruded unilamellar liposomes (LUV) whose lipid compositions mimic roughly the lipid compositions of the respective membrane monolayers. We only use binary and ternary lipid mixtures.

[e] The median substrate binding constant from inner apical membrane monolayer to P-gp

[f] Dissociation constant relative to the cell cytosol, $K_D=1/(K_{PC}*K_C)$.

[g] P refers to the lipid bilayer passive permeability defined as +GF120918. k is the value for the passive permeability through the other transporter for digoxin and loperamide. In reality, the passive permeability coefficients took from 15 min to 6 hrs to reach true steady-state and P_{BA} was not always the same as P_{AB} until the steady-state was reached.

[h] The mass action equations only fit the product K_C*K_{PC}. The partition coefficient for digoxin has not been measured, so we cannot separately estimate the binding constant, K_C, to P-gp or

Table 1 cont'd.

the dissociation rate constant $k_r=k_1/K_C$. We know that the product $K_C\ K_{PC}\sim 3x10^5\ M^{-1}$, data not shown, which yields the K_I shown.

Table 2. SF50 values and Corrections to estimate K_I

Probe-substrate	Inhibitor	SF50 (uM)[a]	Correction Factor from Eq. (8)[b]	K_I Table 1 [c] (uM)	K_I Eq. (8) [d] (uM)
Quinidine	Amprenavir	20	11	5	2
Quinidine	Loperamide	1	11	0.1	0.1
Quinidine	Quinidine	4	11	0.1	0.3
Digoxin	Quinidine	10	5	0.1	2
Digoxin	Verapamil	10	5	ND	2

Legend for Table 2.

[a] IC50 fitted by the standard literature equation, Eq. (3). Experimental data is from this work.

[b] Correction factor calculated using Eq.(8)

[c] The dissociation constant for the inhibitor substrate relative to the cytosol is $K_I=1/(K_{PC}*K_C)$, which is the same as the K_D when the compound is just a substrate, using the parameters in Table 1.

[d] The estimated K_I using the measured IC50 and Eq. (8).

Confluent Monolayer of Polorized Cells

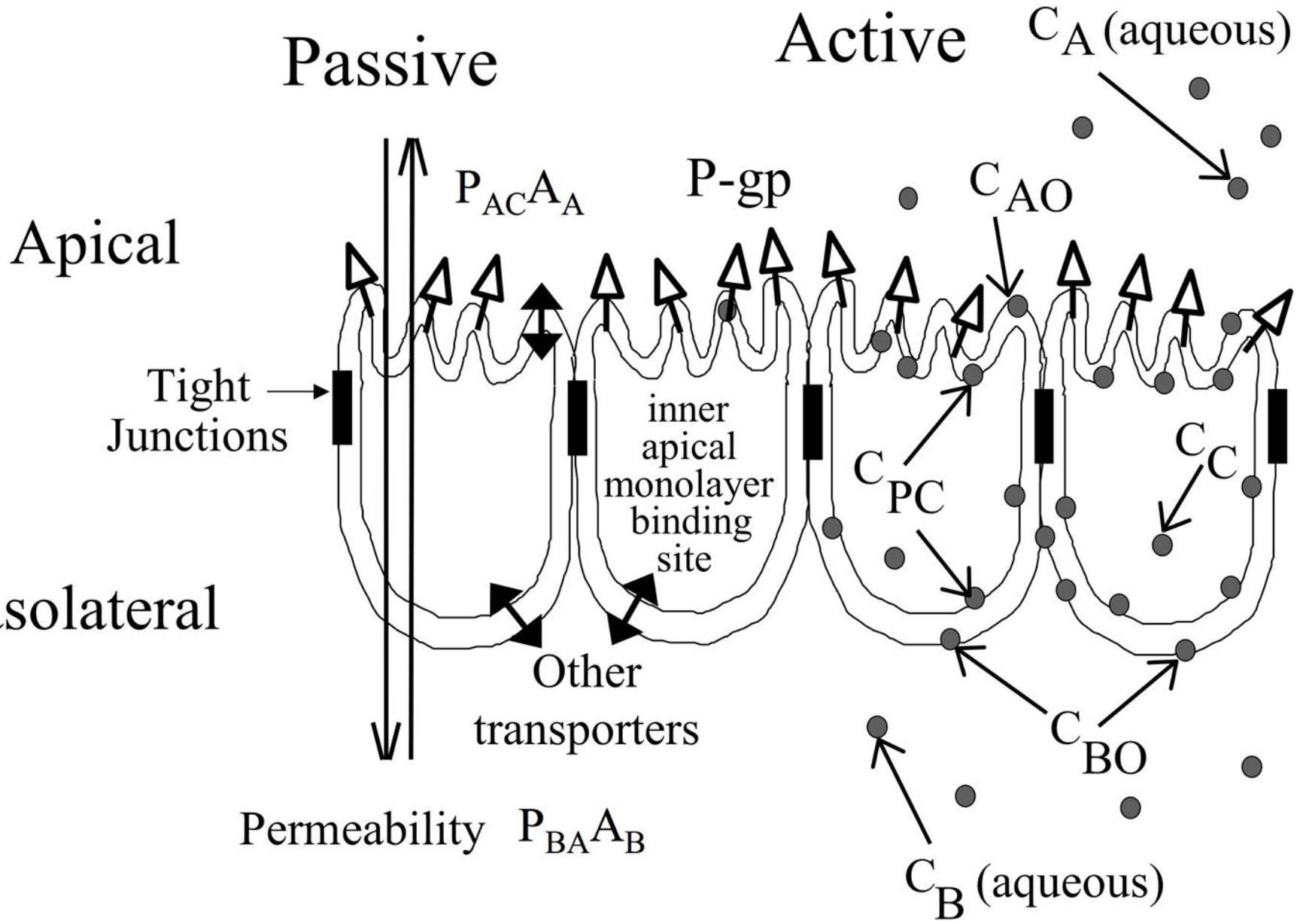

Fig. 1

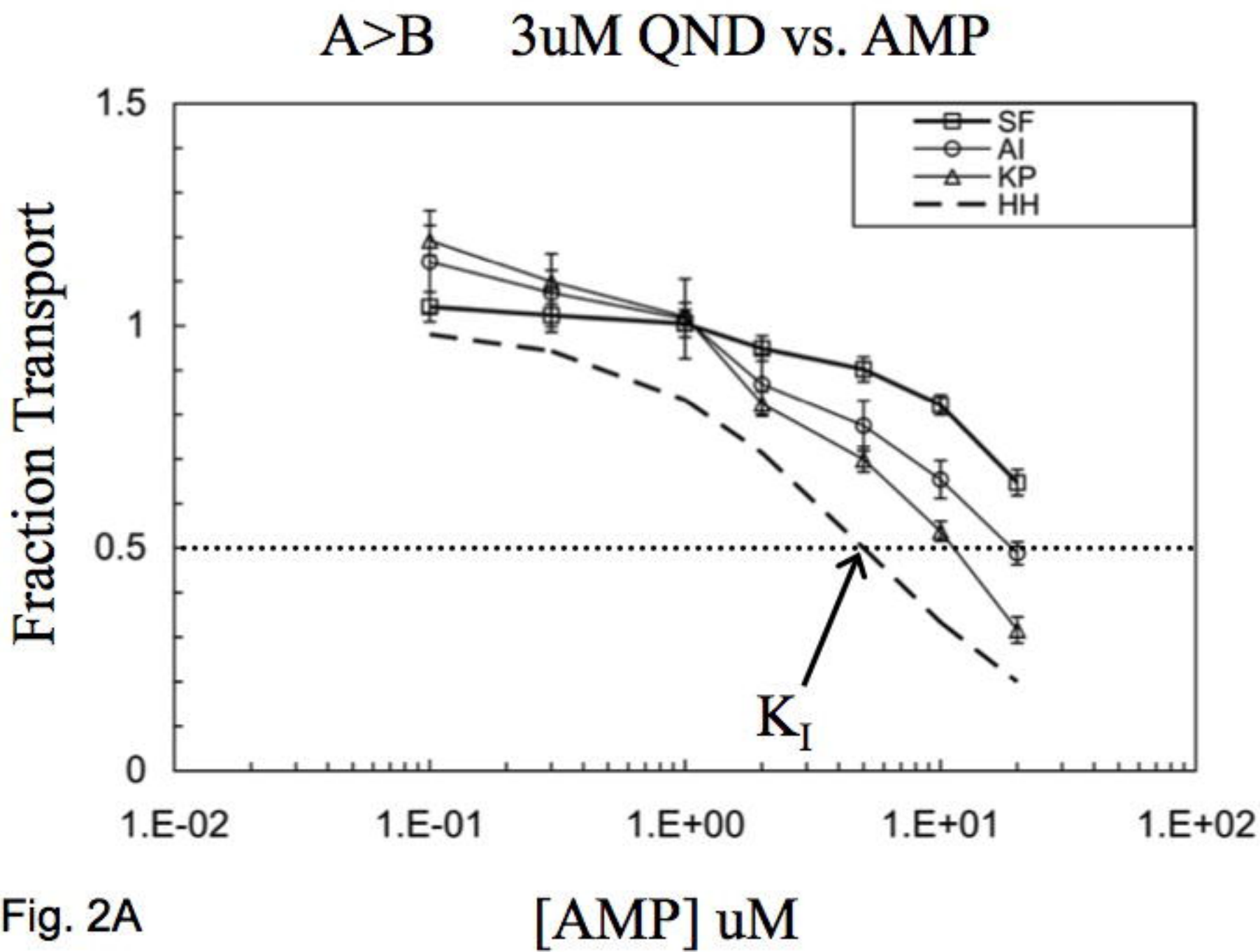
A>B 3uM QND vs. AMP
Fraction Transport
1.5
1
0.5
0
SF
AI
KP
HH
K_I
1.E-02
1.E-01
1.E+00
1.E+01
1.E+02
[AMP] uM

Fig. 2A

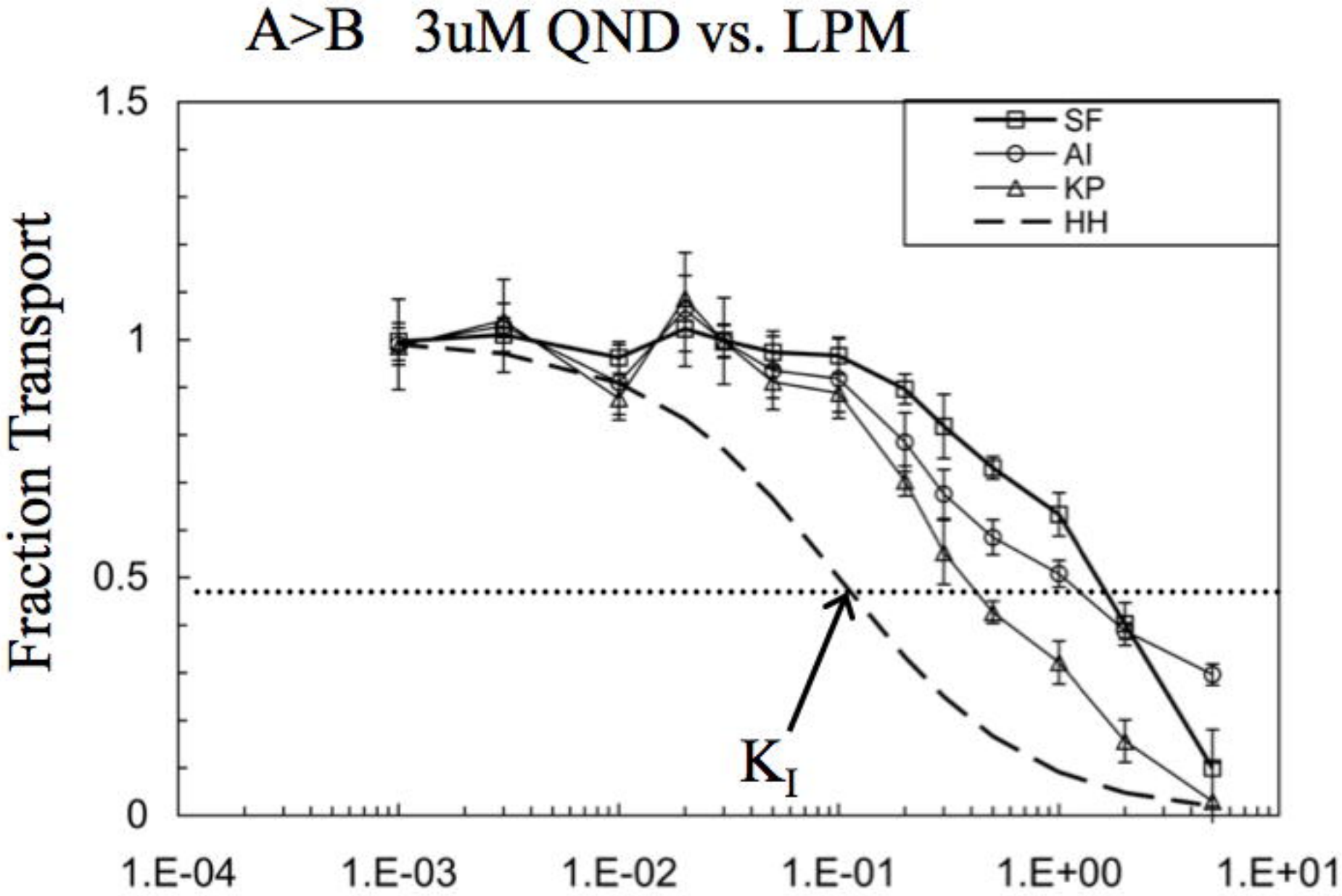
A>B 3uM QND vs. LPM
Fraction Transport
1.5
1
0.5
0
SF
AI
KP
HH
K_I
1.E-04
1.E-03
1.E-02
1.E-01
1.E+00
1.E+01
[LPM] uM

Fig. 2B

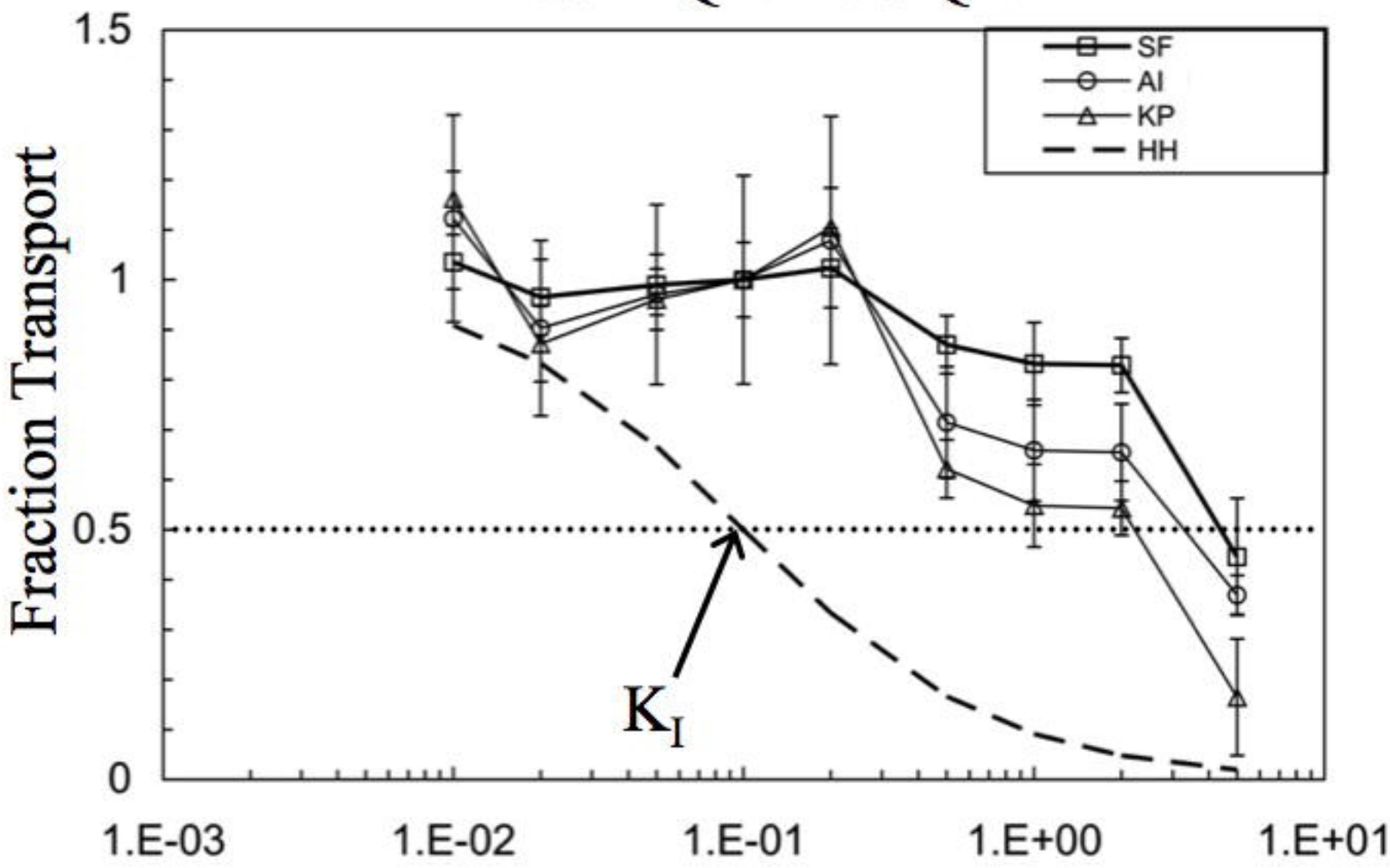
A>B 3uM QND vs. QND
1.5
1
0.5
0
Fraction Transport
SF
AI
KP
HH
K_I
1.E-03
1.E-02
1.E-01
1.E+00
1.E+01
[QND] uM

Fig. 2C

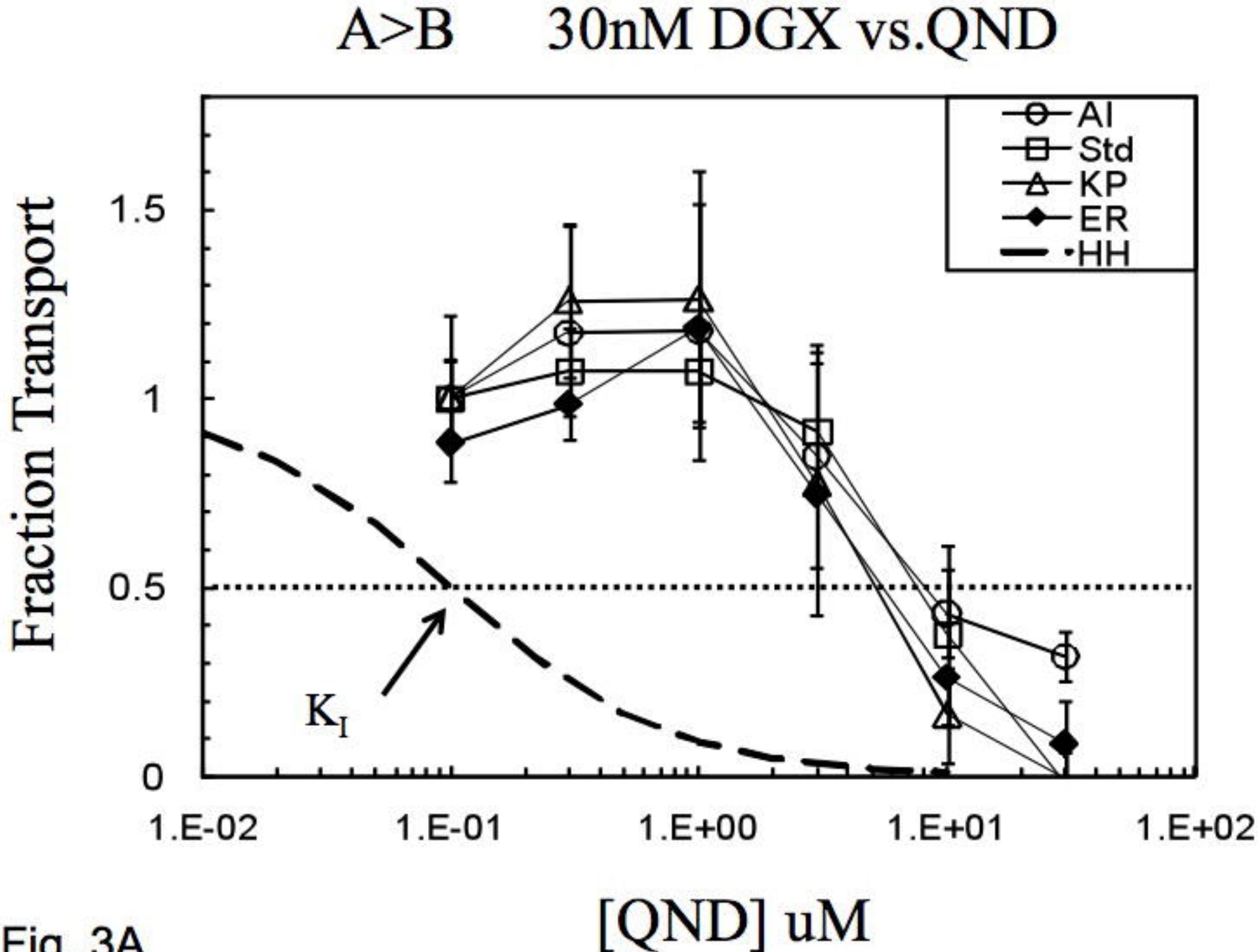
A>B 30nM DGX vs.QND
Fraction Transport
1.5
1
0.5
0
1.E-02
1.E-01
1.E+00
1.E+01
1.E+02
[QND] uM
Al
Std
KP
ER
HH
K_I

Fig. 3A

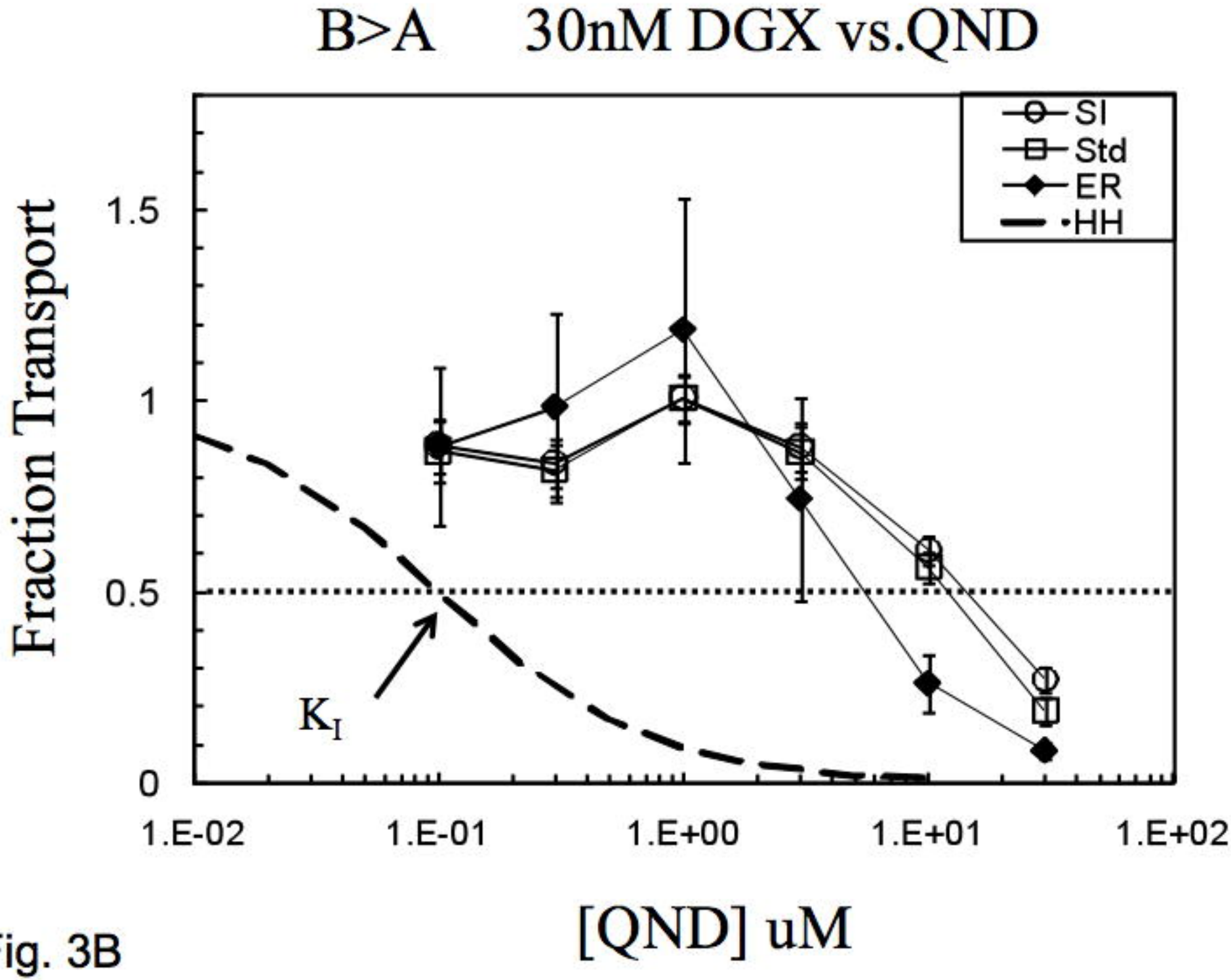
B>A 30nM DGX vs.QND
SI
Std
ER
HH
Fraction Transport
1.5
1
0.5
0
K_I
1.E-02
1.E-01
1.E+00
1.E+01
1.E+02
[QND] uM

Fig. 3B

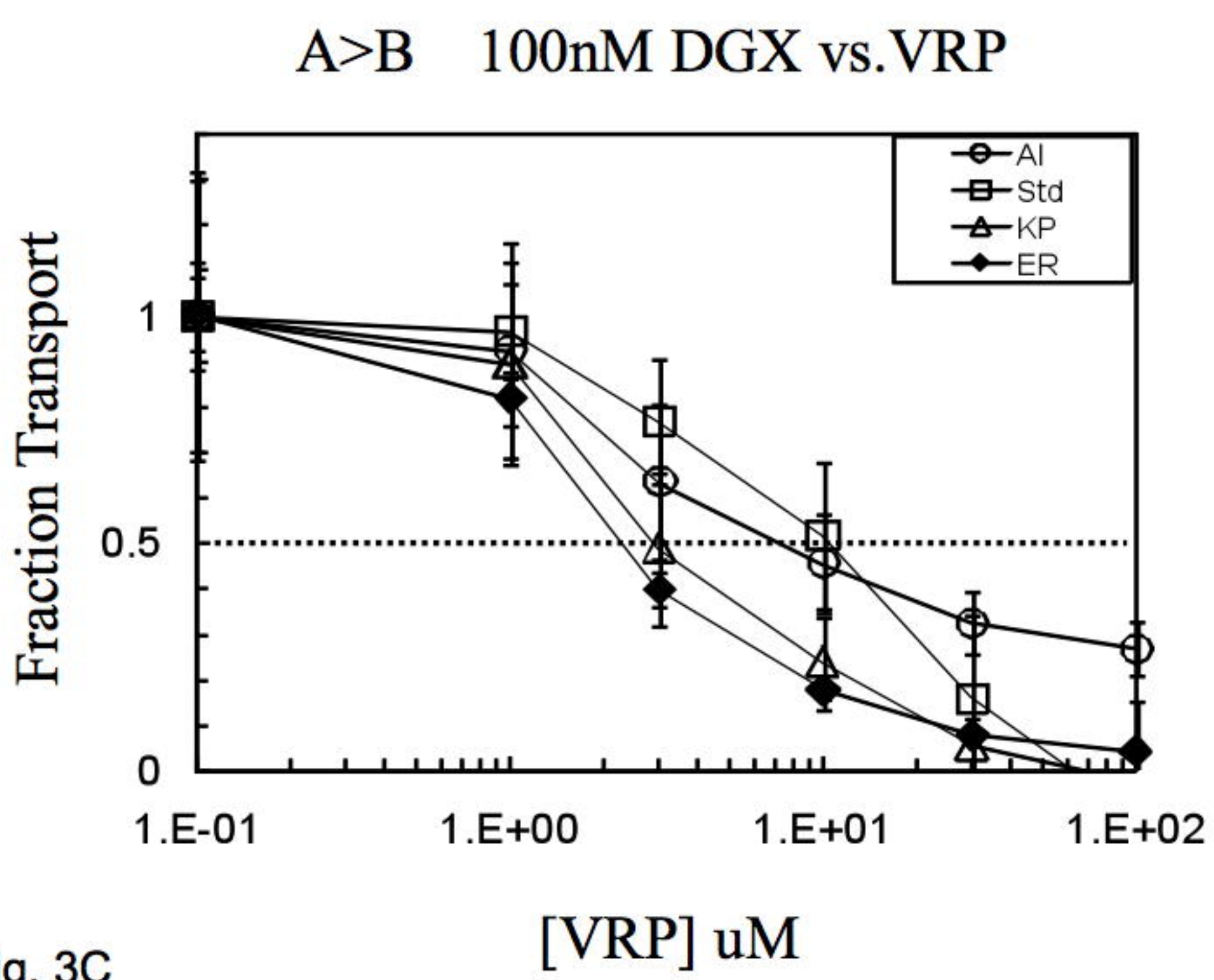
A>B 100nM DGX vs.VRP
Fraction Transport
1
0.5
0
1.E-01
1.E+00
1.E+01
1.E+02
[VRP] uM
AI
Std
KP
ER

Fig. 3C

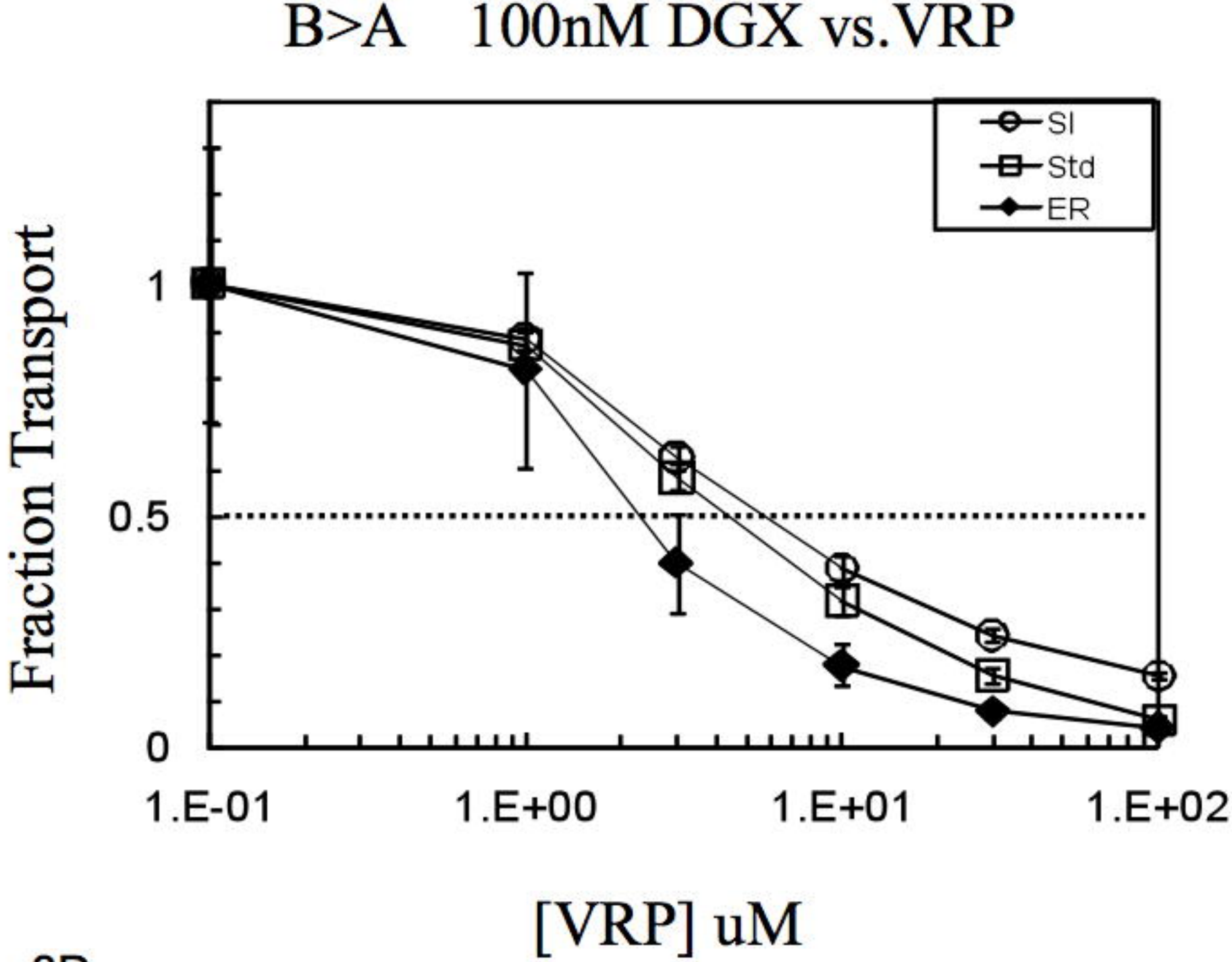
B>A 100nM DGX vs.VRP
SI
Std
ER
Fraction Transport
1
0.5
0
1.E-01
1.E+00
1.E+01
1.E+02
[VRP] uM

Fig. 3D

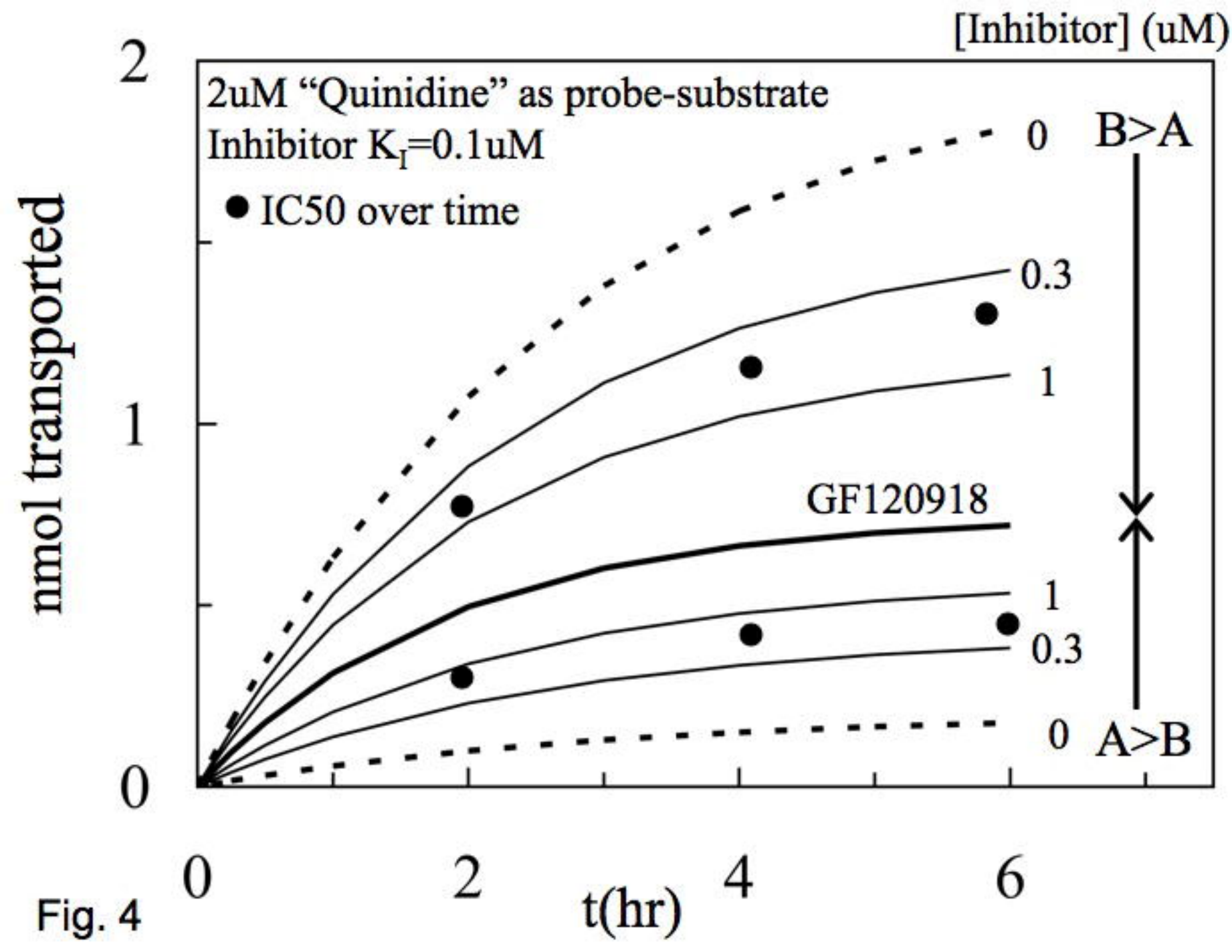
[Inhibitor] (uM)
2uM "Quinidine" as probe-substrate
Inhibitor K_I=0.1uM
IC50 over time
0
0.3
1
GF120918
1
0.3
0
B>A
A>B
nmol transported
2
1
0
0
2
4
6
t(hr)

Fig. 4

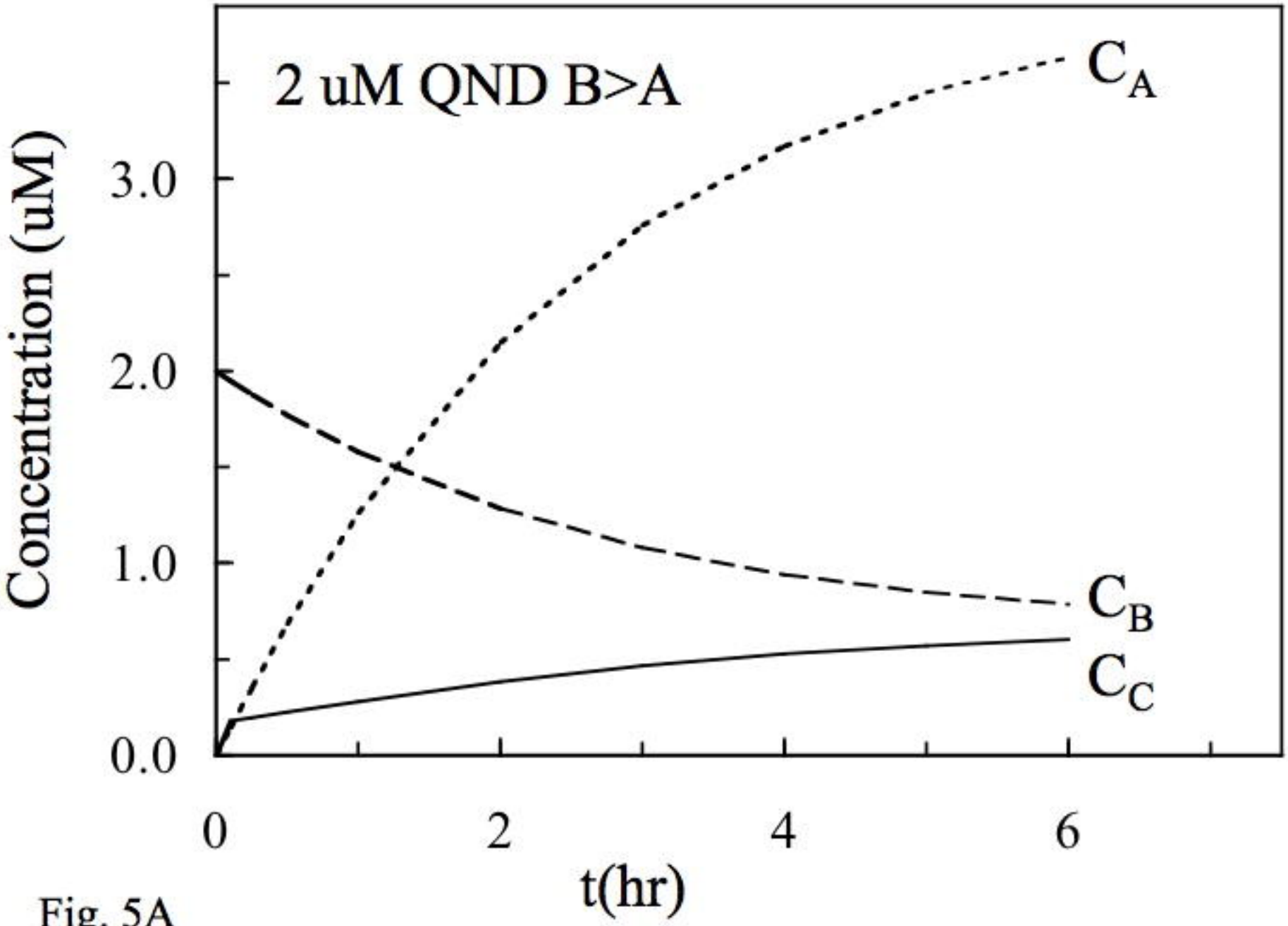

Fig. 5A

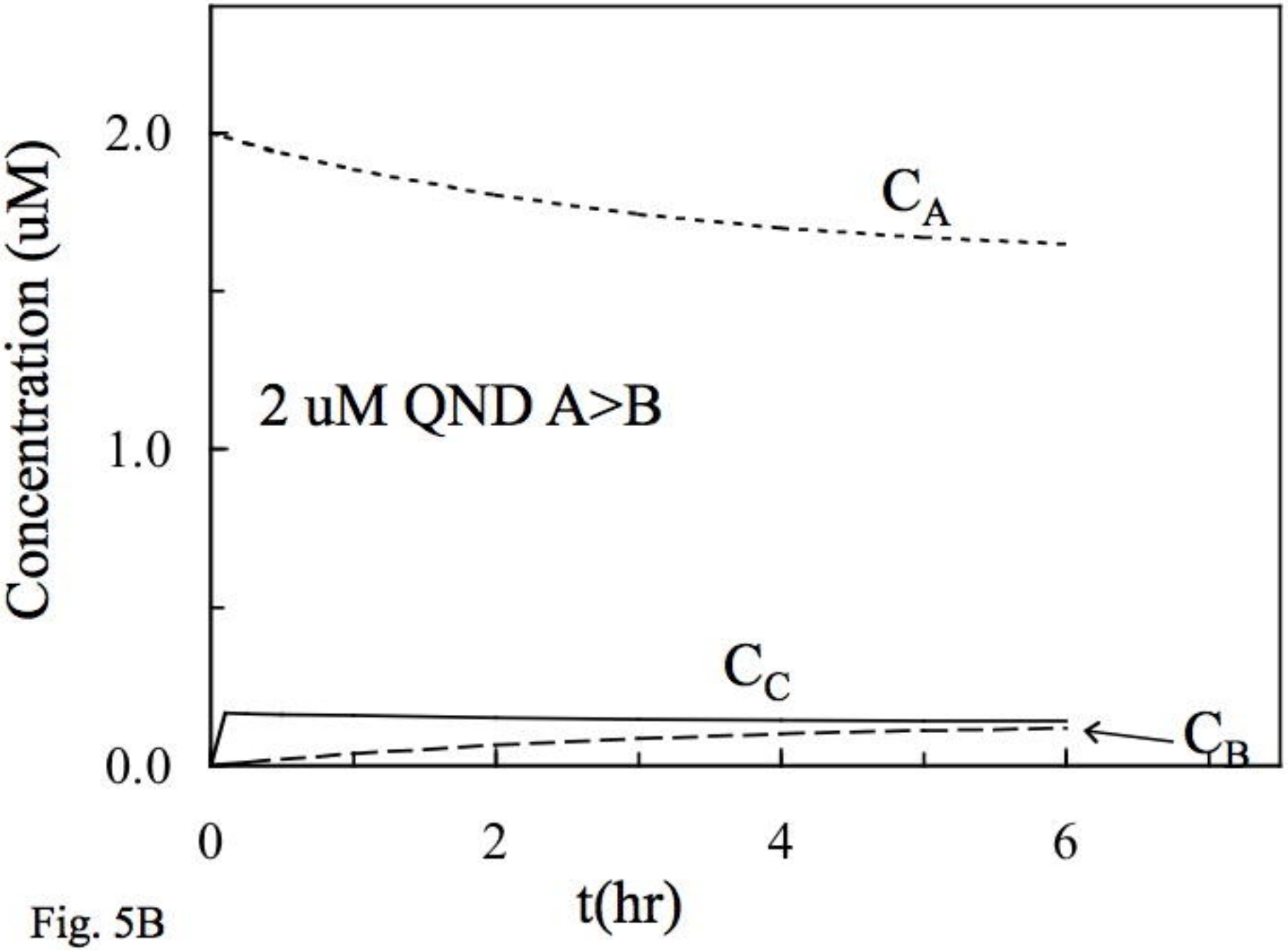

Fig. 5B

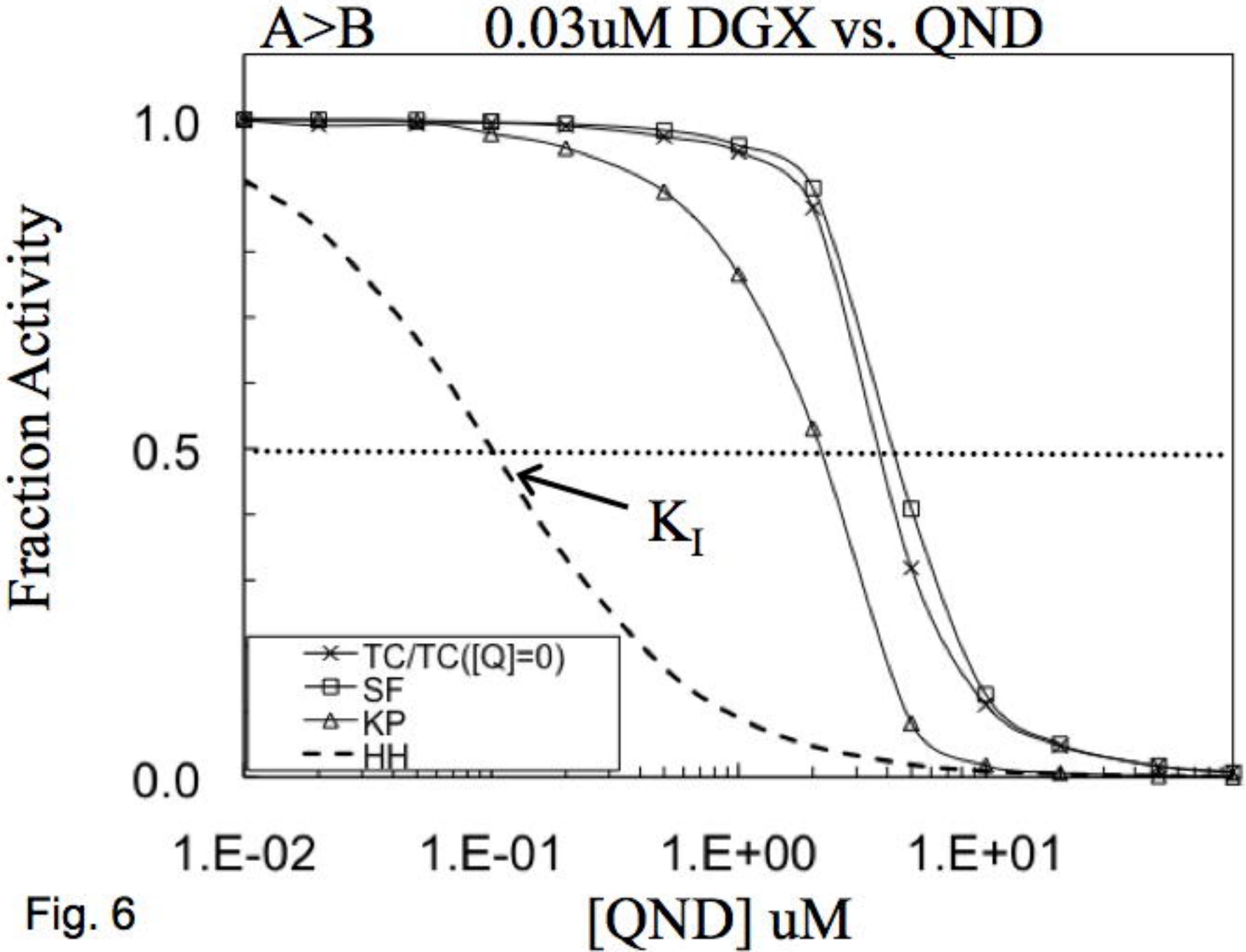
A>B 0.03uM DGX vs. QND
1.0
0.5
0.0
Fraction Activity
K_I
TC/TC([Q]=0)
SF
KP
HH
1.E-02
1.E-01
1.E+00
1.E+01
[QND] uM

Fig. 6

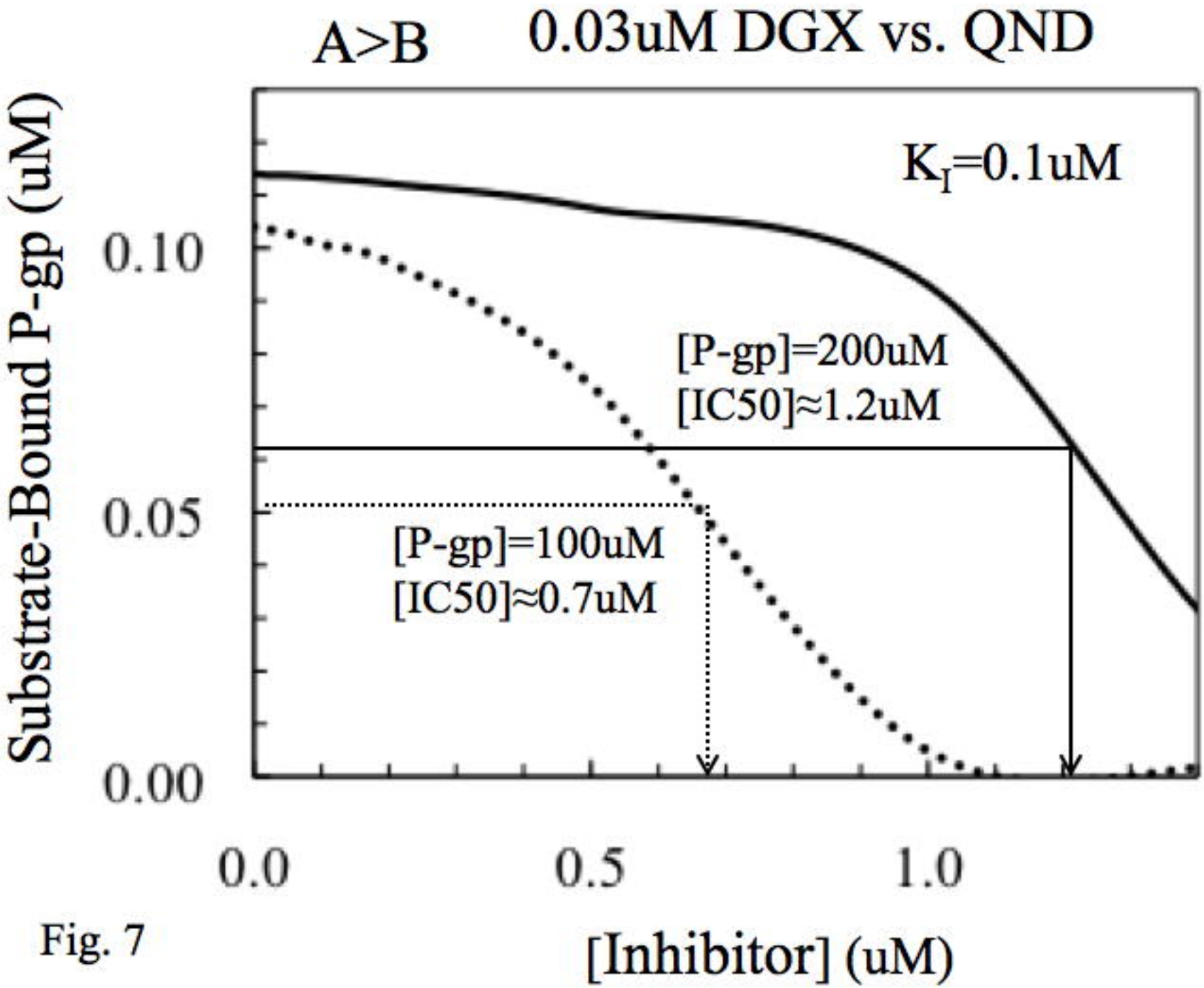
A>B
0.03uM DGX vs. QND
Substrate-Bound P-gp (uM)
0.10
0.05
0.00
K_I=0.1uM
[P-gp]=200uM
[IC50]≈1.2uM
[P-gp]=100uM
[IC50]≈0.7uM
0.0
0.5
1.0
[Inhibitor] (uM)

Fig. 7